Supplementary Material

High-efficiency degradation of norfloxacin by Co-N co-doped biochar synergistically activated peroxymonosulfate: Experiments and DFT calculations

Mingming Ta [a], Tiantian Zhang [a], Tuo Wang [a,*], Juan Guo [a], Rui Yang [a], Jingyu Ren [b], Yanzhong Zhen [b,*], Chunming Yang [c], Chao Bai [c], Yanyan An [a,d], Yufeng Wang [a], Gaihui Liu [e], Fuchun Zhang [e]

[a] School of Architecture and Engineering, Yan'an University, Yan'an 716000, PR China.

[b] Engineering Research Center of Efficient Exploitation of Oil and Gas Resources and Protection Ecological Environment, Universities of Shaanxi Province, Yan'an University, Yan'an 716000, PR China.

[c] School of Chemistry and Chemical Engineering, Yan'an University, Yan'an 716000, PR China.

[d] Department of Civil and Environmental Engineering, The Hong Kong University of Science and Technology, Hong Kong, PR China.

[e] School of Physics and Electronic Information, Yan'an University, Yan'an 716000, PR China.

* Corresponding author

Email: wt@yau.edu.cn; zhenyanzhong@yau.edu.cn

Texts

Text S1. Chemicals

Norfloxacin (NOR, 98%), sulfamethoxazole (SMX, 98%) and ofloxacin (OFX, 98%), atrazine (ATZ, $\geq$ 97%), diclofenac (DCF, 98%), methanol (MeOH, 99.5%), tert-butyl alcohol (TBA, 99%), furfuryl alcohol (FFA, 98%), p-benzoquinone (p-BQ, 99%), L-histidine (L-his, 99%), 5,5-dimethyl-1-pyrroline-N-oxide (DMPO, 97%), 2,2,6,6-tetramethyl-4-piperidinyloxyl (TEMP, > 98%), methyl phenyl sulfone (PMSO$_2$, 98%), methyl phenyl sulfoxide (PMSO, > 98%), dimethyl sulfoxide (DMSO, > 99%), potassium iodide (KI, $\geq$ 99%), potassium peroxymonosulfate (PMS, KHSO$_5$·0.5KHSO$_4$·0.5K$_2$SO$_4$, $\geq$ 42%), and sodium persulfate (PDS, 99%) were purchased from Sigma-Aldrich Company (Shanghai, China). Sulfuric acid (H$_2$SO$_4$, $\geq$ 92.5%), sodium hydroxide (NaOH, 96%), sodium bicarbonate (NaHCO$_3$, $\geq$ 99.8%), sodium dihydrogen phosphate (NaH$_2$PO$_4$·2H$_2$O, 99%), sodium chloride (NaCl, 99.5%), sodium nitrate (NaNO$_3$, 99%), cobalt nitrate hexahydrate (Co(NO$_3$)$_2$·6H$_2$O, 99%), and urea (CH$_4$N$_2$O, 99%) were purchased from Chongqing Dong Chuan Chemical Co., Ltd. (Chongqing, China). All solutions were prepared with deionized water (> 18.2 MΩ cm^{-1} resistivity).

Text S2. Synthesis of Co@NBC

Rice shell was smashed with a plant crusher and sieved through an 80-mesh screen. The powdery was washed with deionized water and dried at 80 °C for 24 h. The product was stored in a sample bottle and used as the feedstock of biochar. Typically, the rice shell powder (3 g) was immersed in a 100 mL mixture of Co(NO$_3$)$_2$·6H$_2$O (3 g) and urea (3 g) solutions, then magnetically stirred at room temperature for 24 h. After that, these suspensions were vacuity filtered and dried at 80 °C for 24 h. Then the samples were pyrolyzed under nitrogen protection in a tube furnace with a heating rate of 5 °C min^{-1} until to 900 °C and then maintained for 2 h. After natural cooling to room temperature, Co and N co-doped biochar (labeled as Co@NBC) had been obtained. For

comparison, biochar (BC) was prepared through calcined at 900°C directly, Co-doped biochar (Co@BC) and N-doped biochar (N@BC) were prepared in the same method without urea or cobalt nitrate hexahydrate, respectively.

Text S3. Co@NBC Characterization

Co@NBC's surface morphology was determined by scanning electron microscopy (SEM, Zeiss Merlin) and transmission electron microscopy (TEM, JEM-2100) at different magnifications. An energy dispersive spectrometer (EDS, SU8010, Hitachi, Japan) was used to measure the chemical elements on the surface of Co@NBC. High-resolution TEM images were recorded using a FEI Tecnai G2 F30 high-resolution transmission electron microscope (HR-TEM). Analyzing the crystal structure of the materials was done by using an X-ray diffractometer (XRD, D/MAX-III A) equipped with nickel-filtered Cu K radiation. In-situ Raman spectra were obtained using a confocal Horiba Scientific LabRAM HR Evolution Raman spectrometer, equipped with a 514 nm laser. The functional group was identified by Flourier transform infrared (FT-IR, Nicolet iS50, Thermo Fisher Scientific). X-ray photoelectron spectroscopy (XPS) (ESCALAB250, Thermo Fisher Inc.) was used to investigate the oxidation status of Co. The Brunauer-Emmette-Teller (BET) specific surface area of each sample was derived from the N_2 adsorption-desorption isotherms (Micromeritics ASAP 2020 system) recorded at 77 K.

Text S4. Analytical methods

In this study, all organic contaminants were detected using high-performance liquid chromatography (HPLC, Waters, USA) with symmetry C18 column (5 μm particle size, 4.6 × 150 mm, Nacalai Tesque, Inc., Japan). NOR (norfloxacin): the mobile phase consisted of formic acid and acetonitrile (60:40, V/V) at a flow rate of 1.0 mL min^{-1}. The detection wavelength was set at 272 nm, and the injection volume was 20 μL.[1] ATZ: the mobile phase consisted of water and methanol (30:70, V/V) at a flow rate of 1.0 mL min^{-1}. The detection wavelength was set at 225 nm, and the injection volume was 20 μL.[2] SMX (sulfamethoxazole): the mobile phase consisted of water (0.1% acetic

acid) and methanol (30:70, V/V) at a flow rate of 1.0 mL min^{-1}. The detection wavelength was set at 266 nm, and the injection volume was 20 μL. OFX (p-nitrophenol): the mobile phase consisted of water and methanol (40:60, V/V) at a flow rate of 1.0 mL min^{-1}. The detection wavelength was set at 294 nm, and the injection volume was 20 μL. DCF: the mobile phase consisted of water (0.1% oxalic acid) and organic phase (acetonitrile: methanol = 2:1) (65:35, V/V) at a flow rate of 1.0 mL min^{-1}. The detection wavelength was set at 230 nm, and the injection volume was 20 μL.[3] Using a TOC-VCPH analyzer (Shimadzu Co., Japan), the mineralization of contaminants was determined in different processes. The decomposition of PMS was detected by the KI method using UV-vis spectrophotometer (UV-5500PC, Shanghai Metash Instruments Co., Ltd, China) at 354 nm.[4] The identification of intermediate products of NOR degradation were performed by an Acquity I-class ultra-performance liquid chromatography coupled to a VION-IMS-QTOF mass spectrometer (UPLC-IMS-QTOF-MS, Waters, Shanghai, China), with a BEH C18 UPLC column (2.1 × 100 mm, 1.7 μm). The residual ionic Co in solution was detected by using ICP-OES 730 (Agilent 700 Series, USA).

Text S5. EPR analysis

The electron paramagnetic resonance (EPR) spectroscopy was evaluated by a Bruker A300 spectrometer (Germany), with 9.44 GHz microwaves with a modulation amplitude of 1.0 G, sweep width of 100 G, modulation frequency = 100 kHz and receiver gain of 1.0×10^4.

Text S6. Electrochemical measurements

All the electrochemical measurements were conducted at room temperature in a standard three-electrode electrochemical cell with an Ag/AgCl (4 M KCl) reference electrode, a platinum wire counter electrode and a catalyst-modified glassy carbon working electrode (0.196 cm, Pine Research Instrumentation, USA), and the electrolyte was a mixture of 50 mM Na$_2$SO$_4$ and 0.5 mM PMS. Homogeneous catalyst ink was first prepared by sonication of 10 mg catalyst powder, 10 mg conductive carbon (Super

P, Alfa Aesar), 0.1 mL Nafion solution (5 wt%, Sigma-Aldrich) and 1 mL absolute ethanol. Then, 3 μL of the as-prepared catalyst ink was pipetted onto the surface of the glassy carbon electrode, leading to a catalyst loading of ∼0.076 mg/cm^2. The catalyst layer was dried in ambient air before use. All the electrochemical data were collected on a CHI 760D electrochemical workstation (Shanghai Chenhua Instrument Co., China). Electrochemical impedance spectra (EIS) were recorded at -0.3 V vs. Ag/AgCl within a frequency range from 10^5 to 10^{-1} Hz using an AC voltage at a 5mV amplitude and the electrolyte was 0.1 M Na_2SO_4. Linear sweep voltammetry (LSV) was measured as the potential from -3.0~3.0 V (vs. Ag/AgCl) with a scanning rate of 50 mV/s. The i-t curves of Co@NBC catalysts obtained at -0.30 V vs. Ag/AgCl using 0.1 M Na_2SO_4 as electrolyte. The changes of open-circuit potentials were carried out with 0.1 M Na_2SO_4 as supporting electrolyte.

Text S7. Density functional theory (DFT) calculation

The Fukui index of NOR was carried out by Gaussian 16 software. The Fukui index based on density functional theory (DFT), which enables natural population analysis (NPA) of neutral molecules and systems with positive and negative charges on the basis of rational optimization of model geometry. And it has been widely used in prediction of reactive sites of nucleophilic (f^+), electrophilic (f^-) and general radical attacks (f^0). The Fukui index can be calculated for the three types of reactions:

Nucleophilic attack:
$$f_A^+ = q_N^A - q_{N+1}^A \tag{S1}$$

Electrophilic attack:
$$f_A^- = q_{N-1}^A - q_N^A \tag{S2}$$

Radical attack:
$$f_A^0 = (q_{N-1}^A - q_{N+1}^A)/2 \tag{S3}$$

where q^A, f, and N represent the atom charge of atom A at the corresponding state, the value of Fukui index, and the number of electrons of NOR, respectively.

The DFT calculations are performed by Vienna Ab initio Simulation Package (VASP) with the projector augmented wave (PAW) method. The exchange-functional is treated using the generalized gradient approximation (GGA) of Perdew-Burke-

Emzerhof (PBE) functional. The energy cutoff for the plane wave basis expansion was set to 500 eV and the force on each atom less than 0.05 eV/Å was set for convergence criterion of geometry relaxation. The Brillourin zone was sampled with Monkhorst mesh 7×7×1 through all the computational process. The self-consistent calculations apply a convergence energy threshold of 10^{-5} eV.
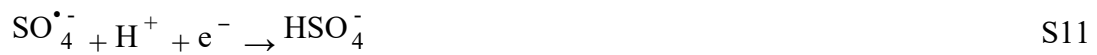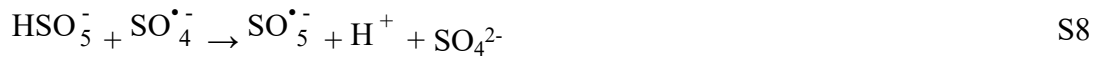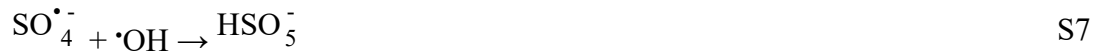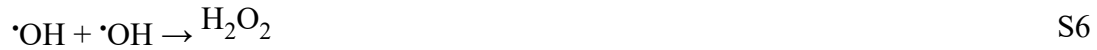
The adsorption energy (E_{ads}) of adsorbate PMS was defined as:

$$E_{ads} = E_{catalyst + PMS} - E_{catalyst} - E_{PMS} \qquad \text{S4}$$

where, $E_{catalyst + PMS}$, $E_{catalyst}$ and E_{PMS} are the energy of adsorbate PMS adsorbed on the catalyst, the energy of clean catalyst, and the energy of isolated PMS atom in a cubic periodic box, respectively.

Text S8. Reaction equations in the Co@NBC system

PMS self-destruction and side reactions:

$$SO_4^{\bullet -} + SO_4^{\bullet -} \rightarrow S_2O_8^{2-} \qquad \text{S5}$$

$$\bullet OH + \bullet OH \rightarrow H_2O_2 \qquad \text{S6}$$

$$SO_4^{\bullet -} + \bullet OH \rightarrow HSO_5^- \qquad \text{S7}$$

$$HSO_5^- + SO_4^{\bullet -} \rightarrow SO_5^{\bullet -} + H^+ + SO_4^{2-} \qquad \text{S8}$$

$$HSO_5^- + \bullet OH \rightarrow SO_5^{\bullet -} + H_2O \qquad \text{S9}$$

$$\bullet OH + H^+ + e^- \rightarrow H_2O \qquad \text{S10}$$

$$SO_4^{\bullet -} + H^+ + e^- \rightarrow HSO_4^- \qquad \text{S11}$$

Linearized Arrhenius equation:

$$ln\ k = ln\ A - E_a/RT \qquad \text{S12}$$

where k is the rate constant (min^{-1}), A is the pre-exponential factor, E_a is the activation energy (kJ mol^{-1}), R is the ideal gas constant (8.314 J mol^{-1} K^{-1}), and T is the absolute temperature (K).

Text S9. Calculation of contribution rate of reactive species

$$R[^{\bullet}OH/SO_4^{\bullet -}] = (k_0 - k_1)/k_0 \qquad \text{S13}$$

$$R[^1O_2] = (k_1 - k_2)/k_0 \qquad \text{S14}$$

$$R[other] = 1 - R[^{\bullet}OH/SO_4^{\bullet -}] - R[^1O_2] \qquad \text{S15}$$

where k_o represented the rate constant of the pristine reaction without any scavenger, k_1 and k_2 were applied as the rate constants of NOR degradation after adding MeOH and FFA, respectively.

Text S10. Inorganic anions reactions

$$Cl^- + SO_4^{\bullet -} \rightarrow Cl^{\bullet} + SO_4^{2-} \qquad \text{S16}$$

$$Cl^- + {}^{\bullet}OH \rightarrow HOCl^{\bullet -} \qquad \text{S17}$$

$$Cl^- + Cl^{\bullet} \rightarrow Cl_2^{\bullet -} \qquad \text{S18}$$

$$HCO_3^- + {}^{\bullet}OH \rightarrow CO_3^{\bullet -} + H_2O \qquad \text{S19}$$

$$HCO_3^- + SO_4^{\bullet -} \rightarrow HCO_3^{\bullet} + SO_4^{2-} \qquad \text{S20}$$

$$CO_3^{\bullet -} + O_2^{\bullet -} \rightarrow CO_3^{2-} + O_2 \qquad \text{S21}$$

$$NO_3^- + {}^{\bullet}OH \rightarrow NO_3^{\bullet} + OH^- \qquad \text{S22}$$

$$NO_3^- + SO_4^{\bullet -} \rightarrow NO_3^{\bullet} + SO_4^{2-} \qquad \text{S23}$$
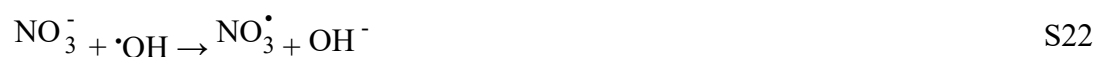
Tables

Table S1. The surface area and pore structure parameters of the samples.

Samples	BET surface area (m^2/g)	Micropore surface area (m^2/g)	Total pore volume (cm^3/g)	micropore volume (cm^3/g)	Average pore diameter (nm)
BC	125.8002	85.0986	0.10195	0.06799	5.2544
N@BC	156.0683	118.6687	0.18251	0.10535	4.9145
Co@BC	199.3458	155.1566	0.21321	0.144752	4.7556
Co@NBC	325.3775	235.6898	0.37757	0.219216	4.9392
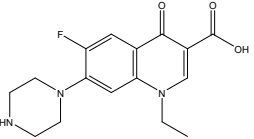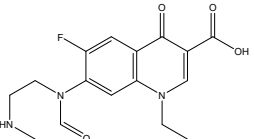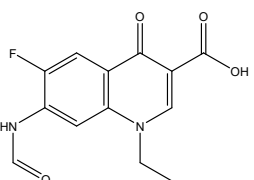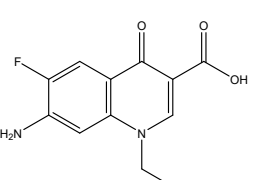
Table S2. Comparison between Co@NBC/PMS system and the previously reported methods in the NOR degradation and kinetic constant.
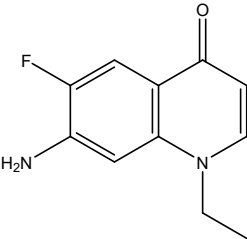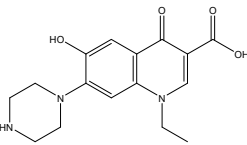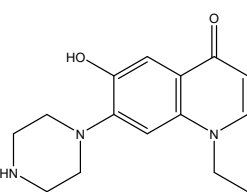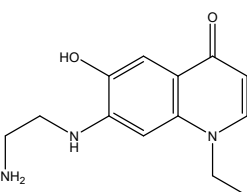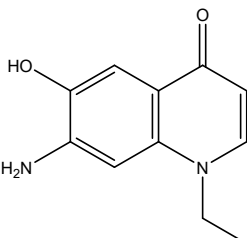
Process	Pollutant	Concentration (mg L^{-1})	Catalyst doses (g L^{-1})	Degradation efficiency	Kinetic constant (min^{-1})	Ref.
CuFe$_2$O$_4$/PMS	NOR	8	0.2	> 90% in 120 min	0.039	5
MGA/PDS	NOR	20	0.15	98.7% in 90 min	0.0487	6
Fe@N co-doped BC/PDS	NOR	10	0.1	95% in 80 min	0.258	7
RSB/E/PMS	NOR	10	1	90.58% in 40 min	0.0584	8
MCAC/E/PMS	NOR	10	1	90.81% in 60 min	0.0515	9
MnFe$_2$O$_4$/H$_2$O$_2$	NOR	10	0.6	90.6% in 90 min	0.02	10
MnCo$_2$-190/Light	NOR	15	0.3	91.78% in 30 min	0.0685	11
Co@NBC-PMS	NOR	10	0.1	94.45% in 40 min	0.341	This work
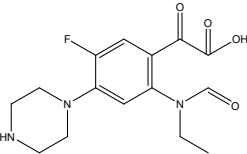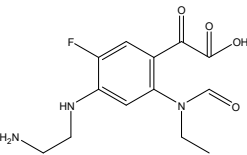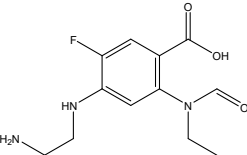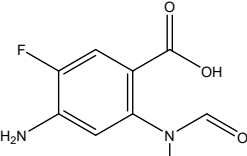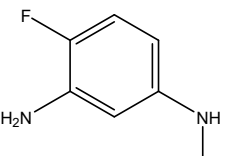
Table S3. The rate constants of ROS with probe compounds.

Organic	$k_{SO_4^{\bullet-}}$ (M⁻¹ s⁻¹)	$k_{\bullet OH}$ (M⁻¹s⁻¹)	k_{1O2} (M⁻¹ s⁻¹)	$k_{O_2^{\bullet-}}$ (M⁻¹s⁻¹)	References
TBA	4×10^5	6×10^8	3.04×10^3	—	12
MeOH	1.1×10^7	9.7×10^8	3.89×10^3	—	12
p-BQ	—	1.2×10^9	—	2.9×10^9	13
L-his	2.5×10^9	7.1×10^9	3.2×10^7	—	12
FFA	1.3×10^{10}	1.5×10^{10}	1.2×10^8	3.5×10^3	14

Table S4. Acute and chronic toxicity of NOR and its oxidation intermediates assessed by ECOSAR V 2.0.

No.	Formula	Structural formula	Acute toxicity (mg/L)			Chronic toxicity (mg/L)		
			Fish (LC$_{50}$)	Daphnid (LC$_{50}$)	Green Algae (EC$_{50}$)	Fish (ChV)	Daphnid (ChV)	Green Algae (ChV)
NOR 320	C$_{16}$H$_{18}$FN$_3$O$_3$		20100	1830	2570	2650	116	703
M1 336	C$_{16}$H$_{18}$FN$_3$O$_4$		111000	8920	16100	21600	499	4020
M2 279	C$_{13}$H$_{11}$FN$_2$O$_4$		16900	15400	7440	7800	1900	1560
M3 251	C$_{12}$H$_{11}$FN$_2$O$_3$		1360	49	154	21.2	0.541	65.4

Compound	Formula						
M4 206	$C_{11}H_{11}FN_2O$	412	309	169	145	43.6	46.2
M5 318	$C_{16}H_{19}N_3O_4$	55900	4710	7720	9370	276	2000
M6 274	$C_{15}H_{19}N_3O_2$	95.9	31.7	8.25	8.94	3.13	15.2
M7 248	$C_{14}H_{17}N_3O_2$	458	45.9	53.4	45.3	3.18	15.6
M8 205	$C_{10}H_{12}N_2O_2$	150	40.3	12.7	13.4	3.66	20.9

M9 324	C$_{15}$H$_{18}$FN$_3$O$_4$		363	397	33.3	3.38	49.5	15.1
M10 298	C$_{13}$H$_{16}$FN$_3$O$_4$		1690	2110	111	10.6	189	33.8
M11 270	C$_{12}$H$_{16}$FN$_3$O$_3$		3200	3520	290	29.4	433	130
M12 227	C$_{10}$H$_{11}$FN$_2$O$_3$		1240	1270	131	13.7	184	70.9
M13 154	C$_8$H$_{11}$FN$_2$		94.6	3.16	10.1	1.52	0.035	4.42

Note: For acute toxicity, $LC_{50} > 100$ or $EC_{50} > 100$ is harmless, $10 < LC_{50} < 100$ or $10 < EC_{50} < 100$ is harmful, $1 < LC_{50} < 10$ or $1 < EC_{50} < 10$ is toxic, and $LC_{50} < 1$ or $EC_{50} < 1$ is highly toxic. For chronic toxicity, $ChV > 10$ is harmless, $1 < ChV < 10$ is harmful, $0.1 < ChV < 1$ is toxic, and $ChV < 0.1$ is highly toxic.

Table S5. Water quality parameters of the tap water and surface water.

	Yanhe River	Lake water	Tap water
pH	7.84	9.15	7.09
UV_{254}	0.09	0.18	0.04
DOC (mg/L)	35.97	62	1.28
CO_3^{2-} (mg/L)	0.76	1.18	0.38
HCO_3^- (mg/L)	113.84	180.41	103
Cl^- (mg/L)	6.05	2.01	10.5
NO_3^- (mg/L)	4.48	1.32	2.05
SO_4^{2-} (mg/L)	50.96	5.02	55.17
PO_4^{2-} (mg/L)	2.49	4.02	1.12

Table S6. The loss ratio of catalyst after collection.

Catalyst	1 st	2 nd	3 rd	4 th	5 th	6 th	7 th	8 th	9 th	10 th
Co@NBC	2.15%	2.52%	2.72%	3.11%	3.42%	3.71%	3.95%	4.13%	4.36%	4.74%
Co@BC	2.04%	2.41%	2.87%	3.27%	3.59%	3.82%	4.15%	4.33%	4.57%	4.89%

Figures
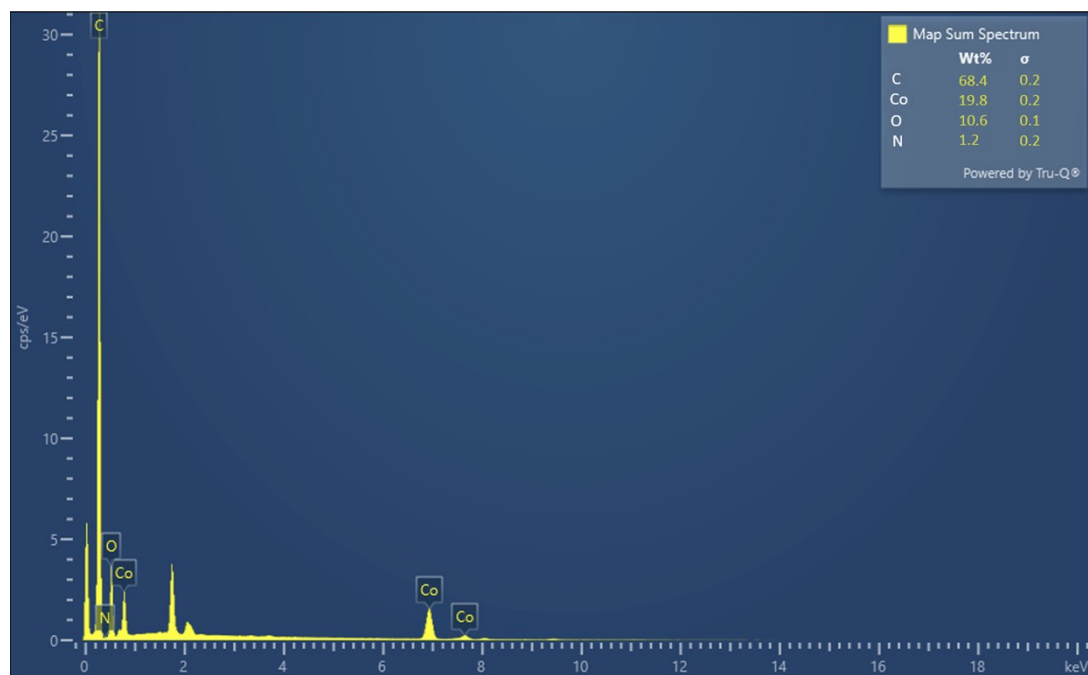
Fig. S1 EDS analysis of Co@NBC.
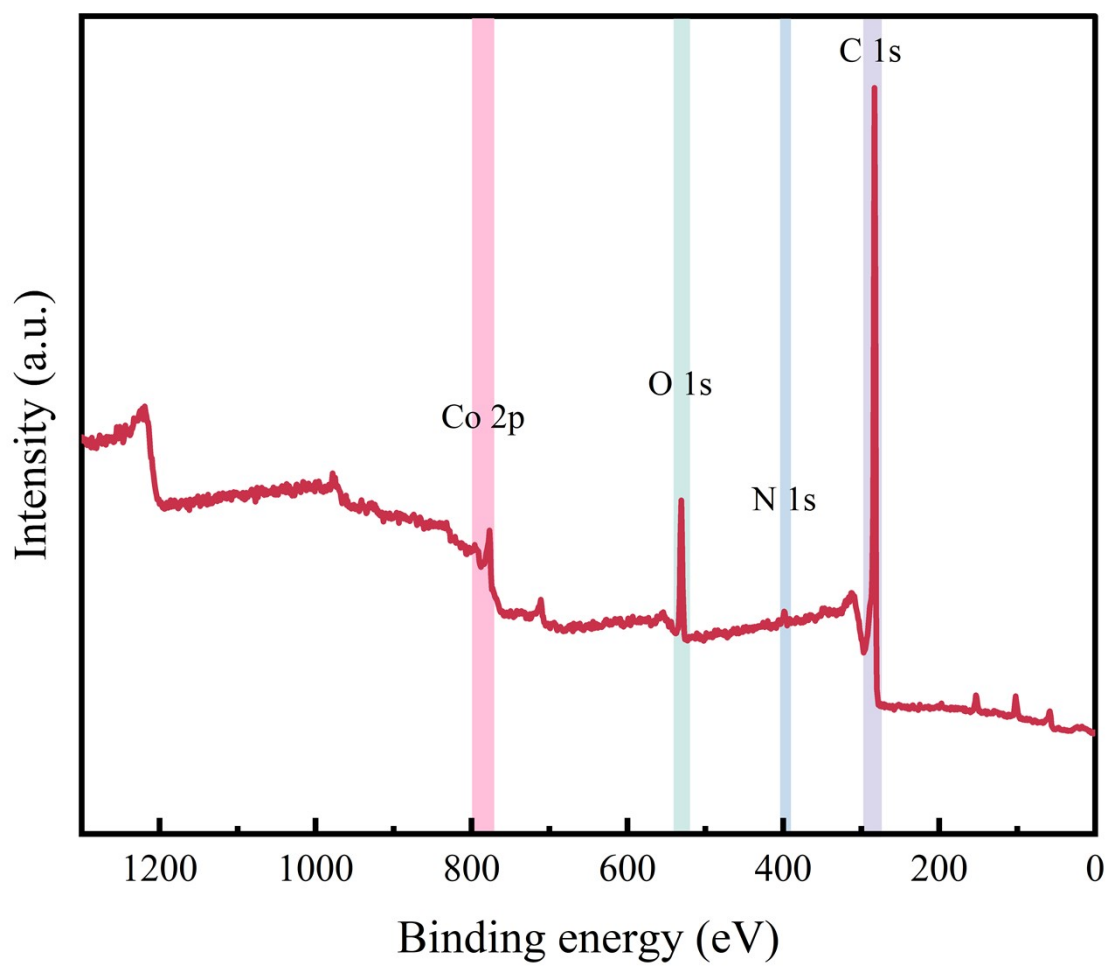
Fig. S2 XPS full-spectrum of fresh Co@NBC.
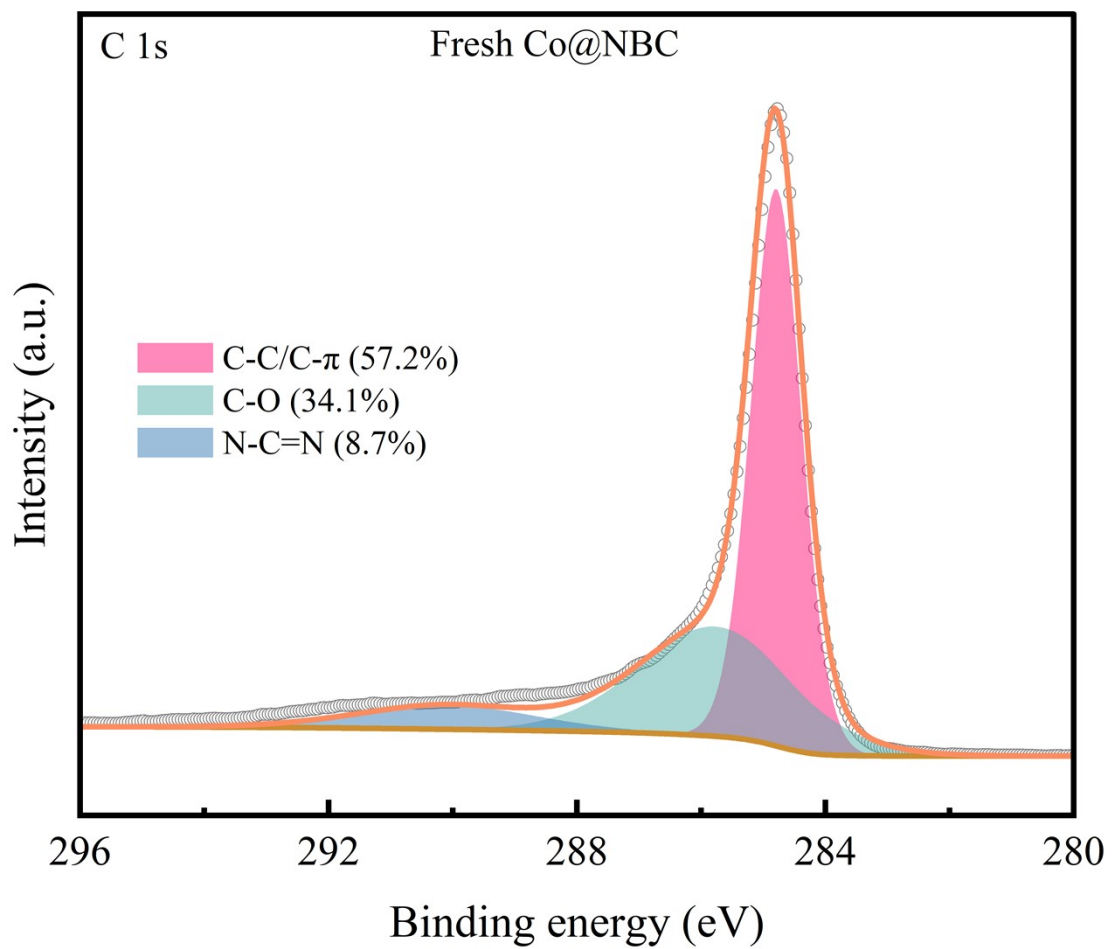
Fig. S3 C 1s XPS spectra of fresh Co@NBC.
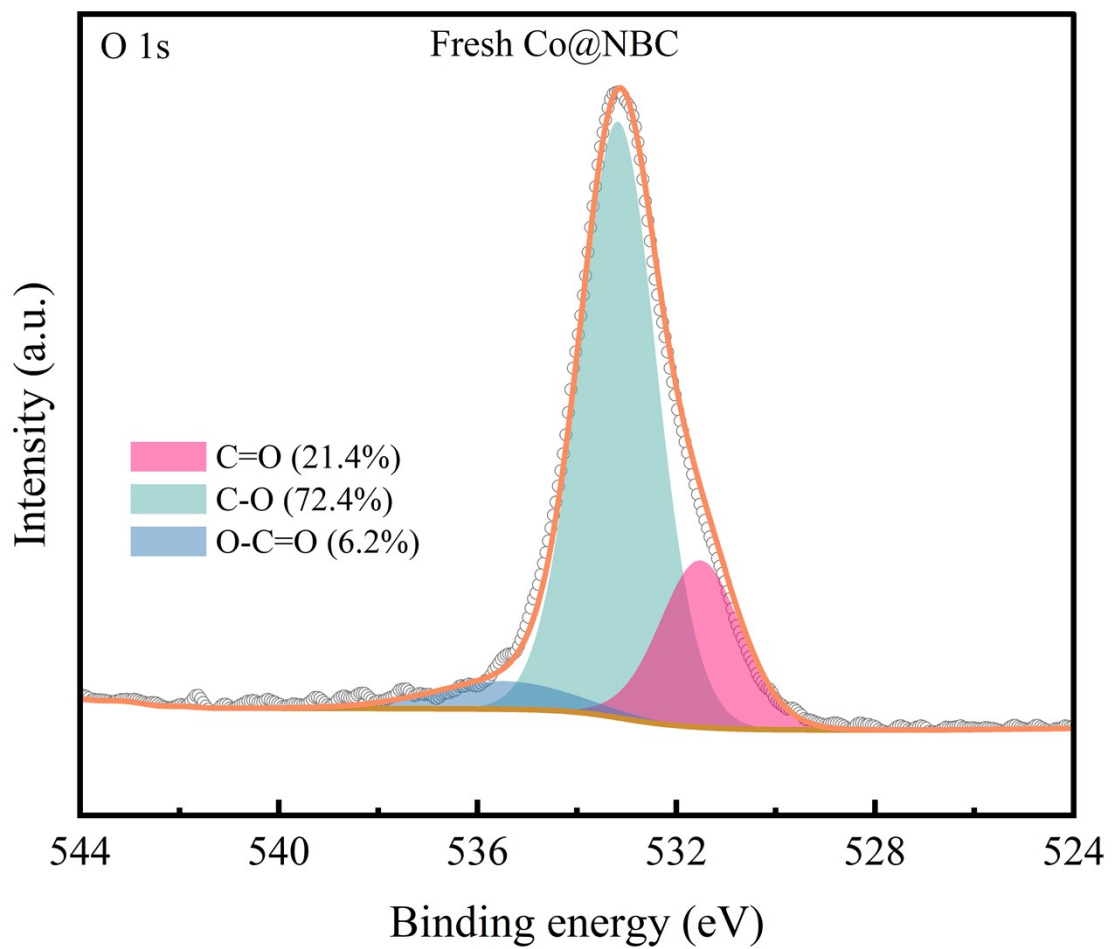
Fig. S4 O 1s XPS spectra of fresh Co@NBC.
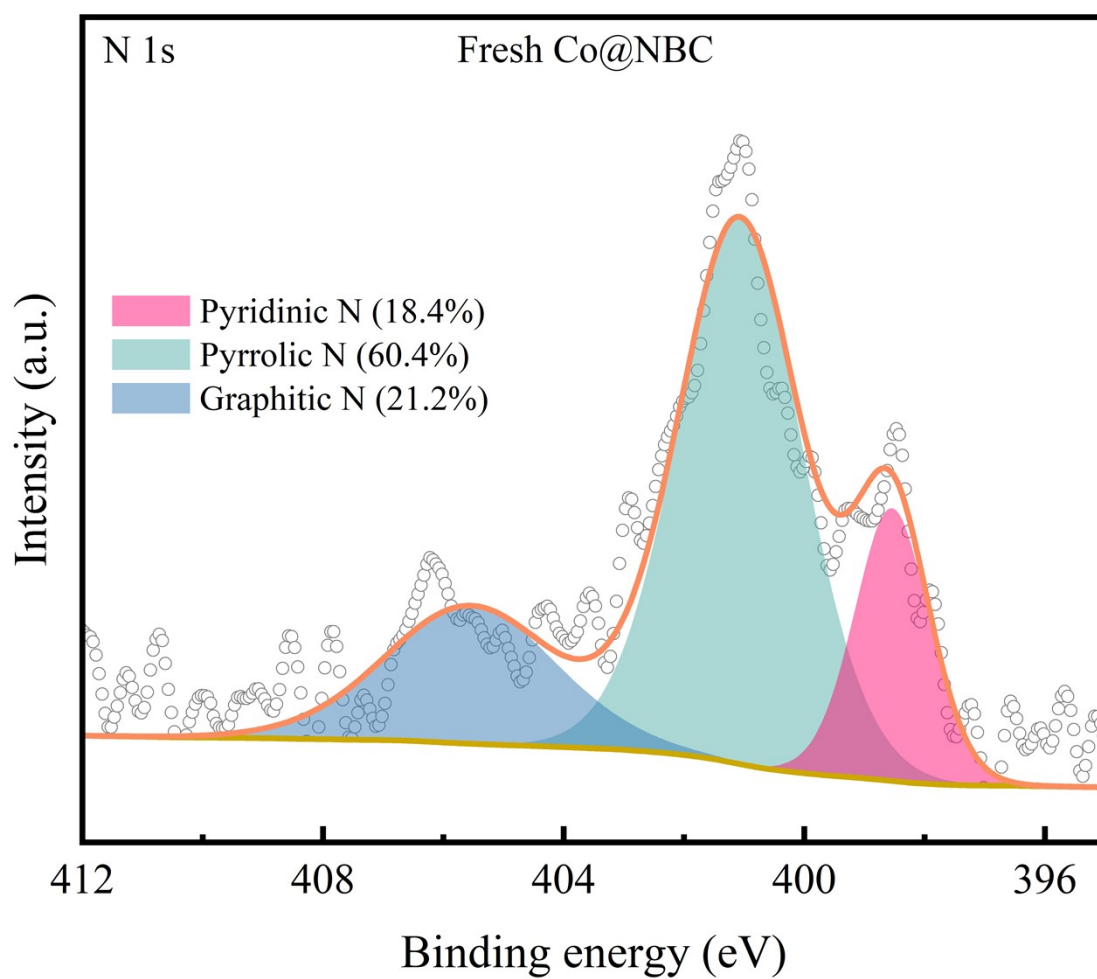
Fig. S5 N 1s XPS spectra of fresh Co@NBC.
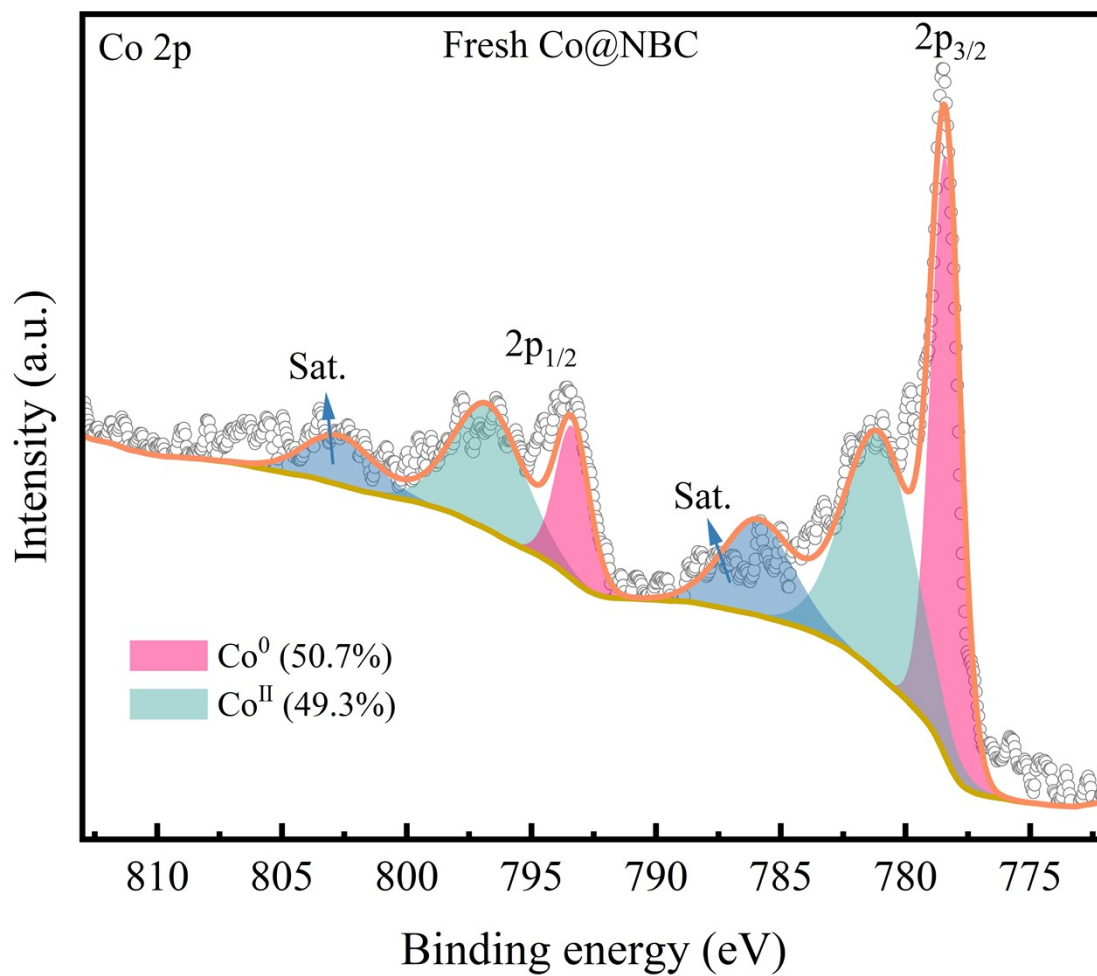
Fig. S6 Co 2p XPS spectra of fresh Co@NBC.
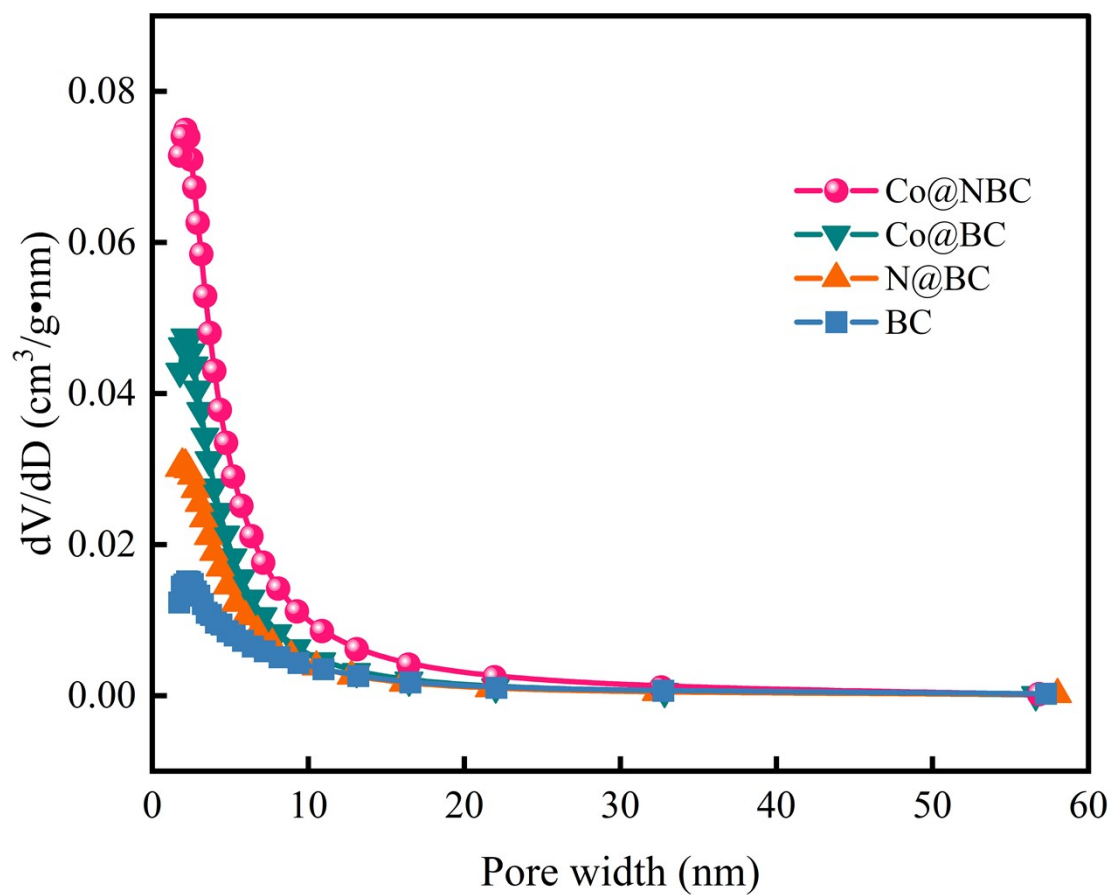
Fig. S7 Pore-size distribution plots of the Co@NBC, Co@BC, N@BC, and BC.
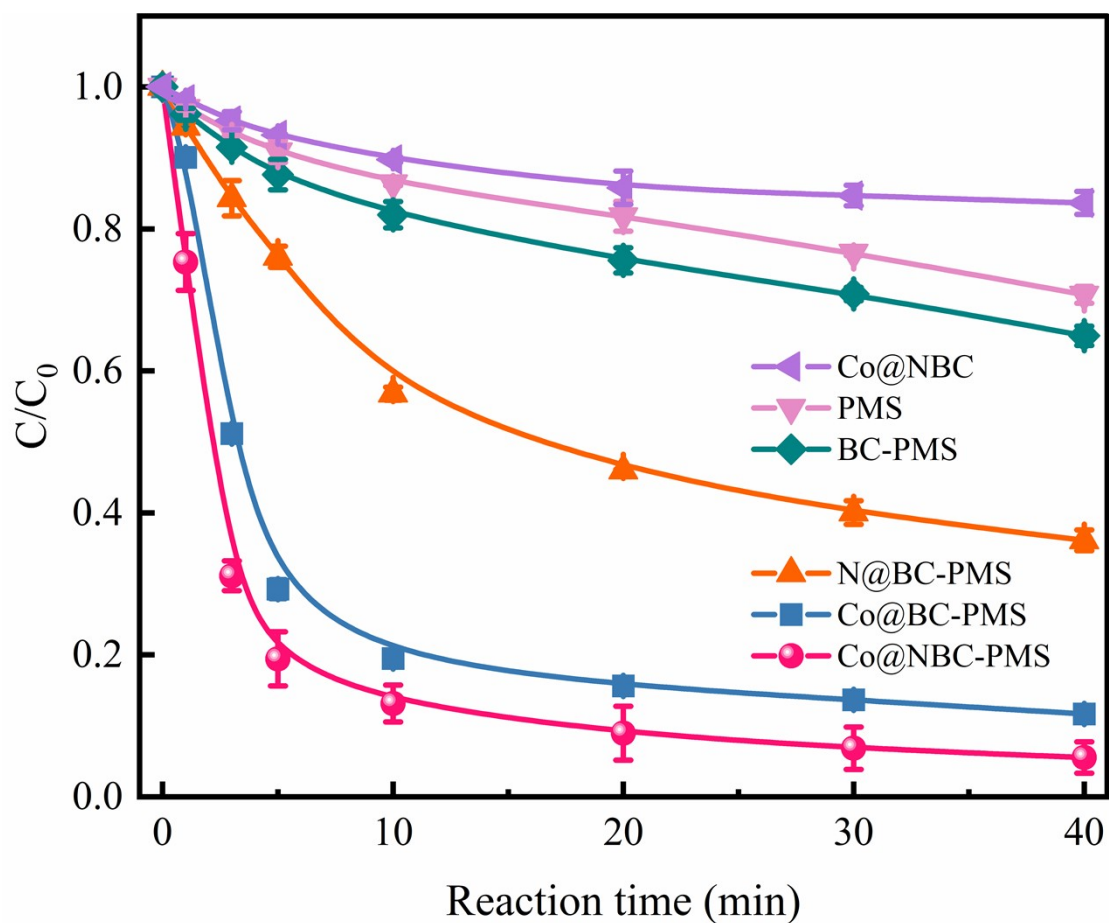
Fig. S8 Comparison of the NOR degradation efficiencies in different systems.
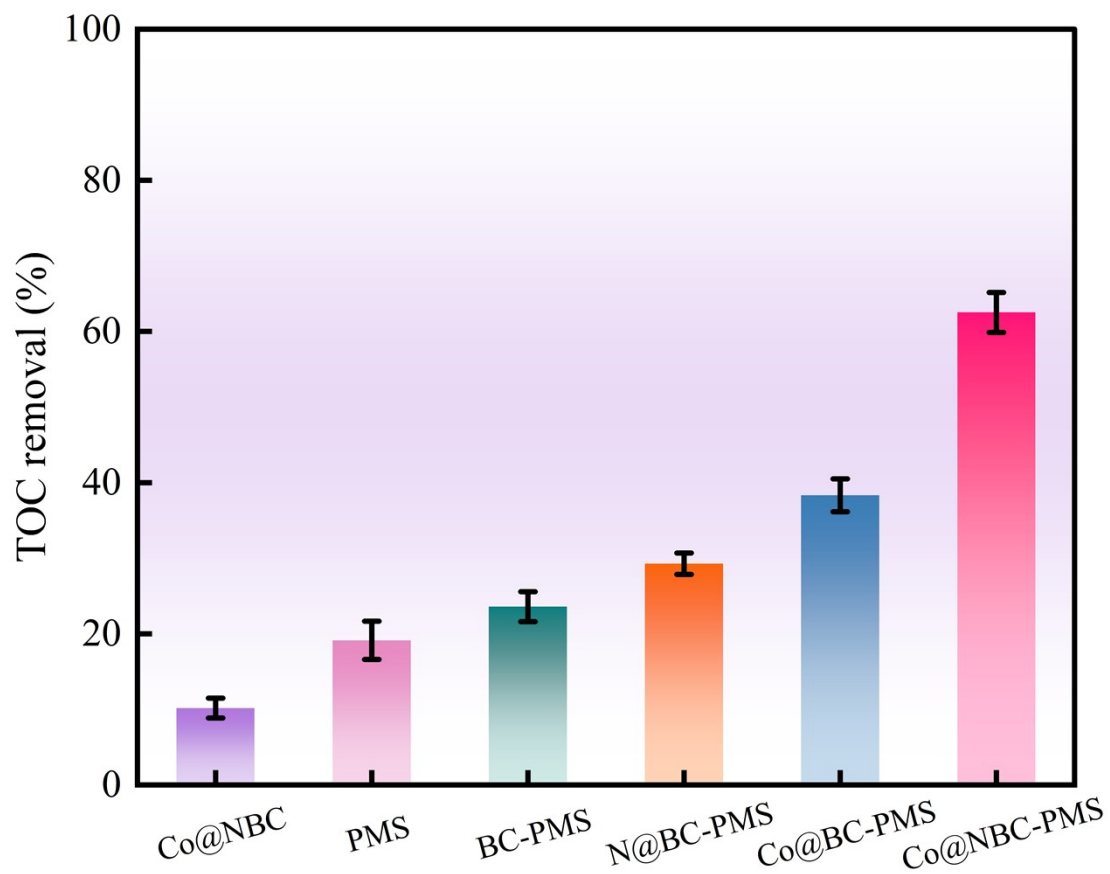
Fig. S9 TOC removal in different catalytic systems.
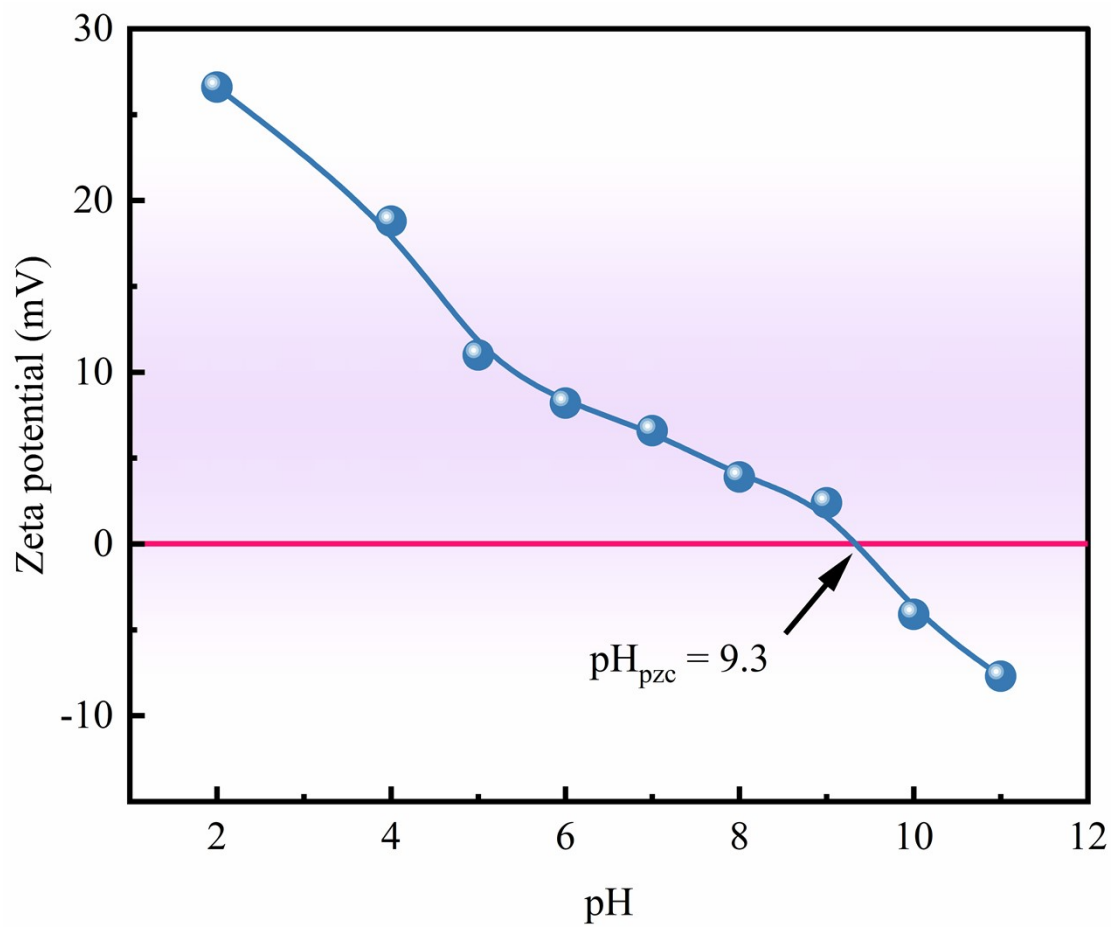
Fig. S10 Zeta potential of Co@NBC.
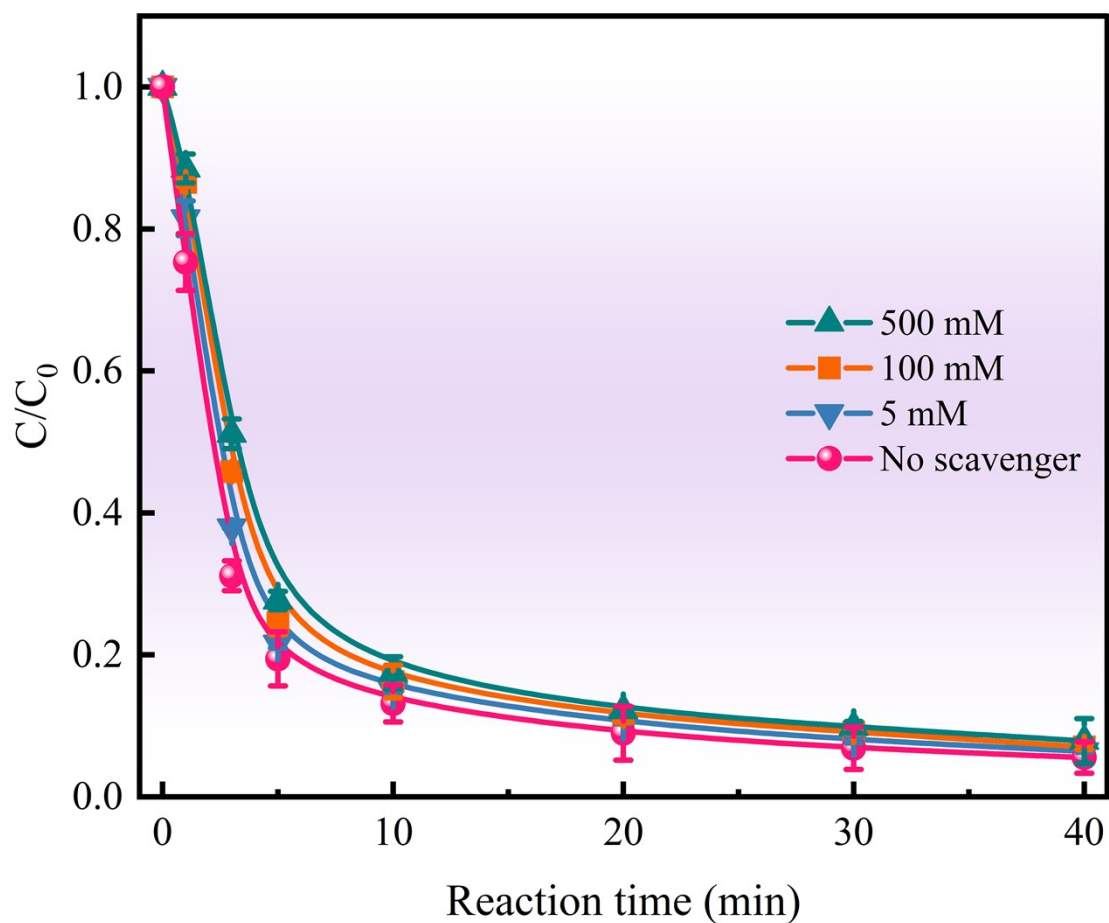
Fig. S11 Effect of concentration of TBA on the removal rate of NOR in the Co@NBC-PMS system.
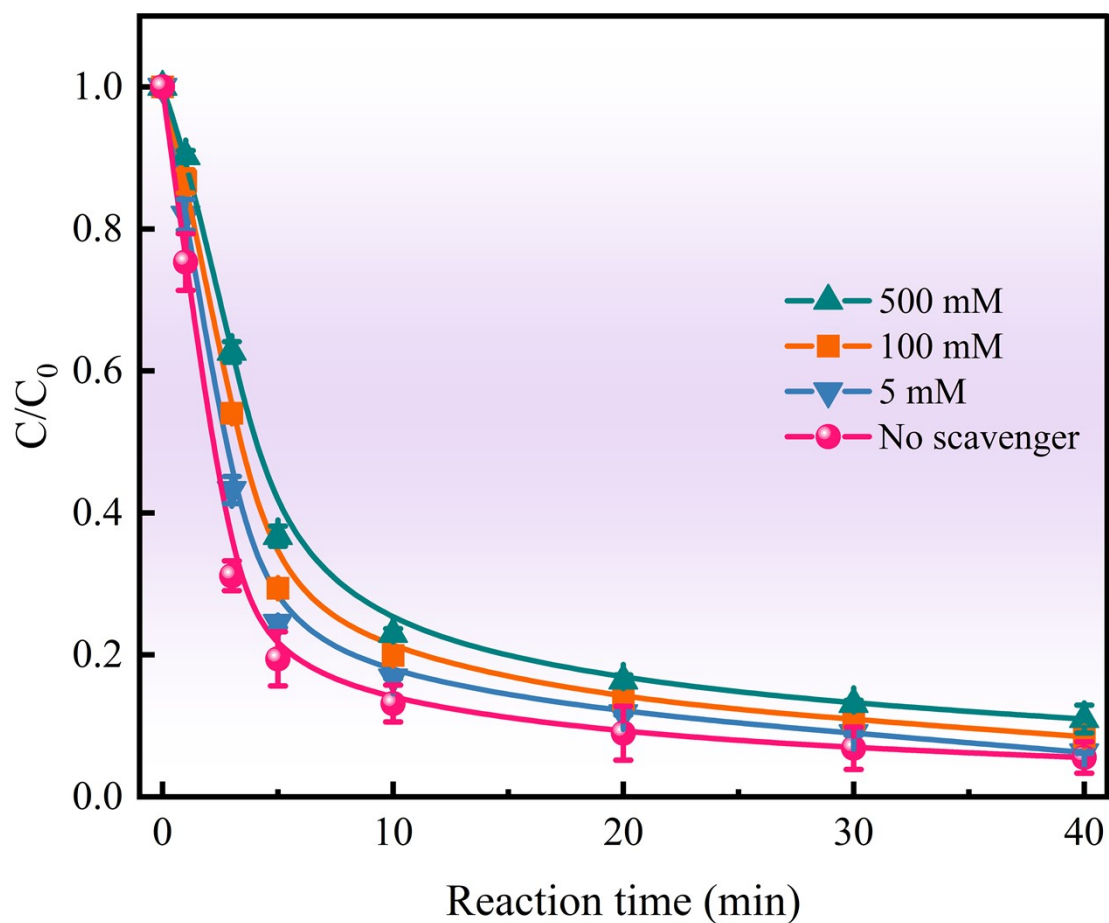
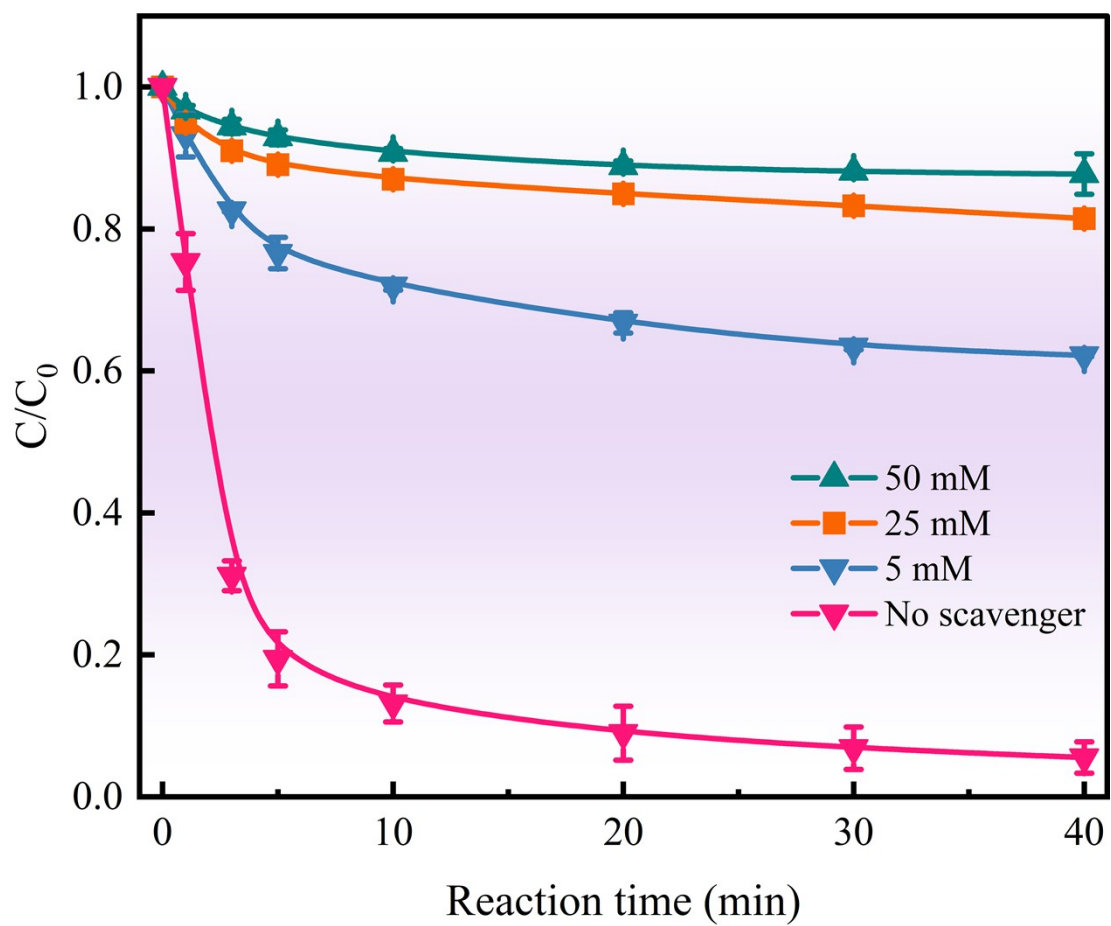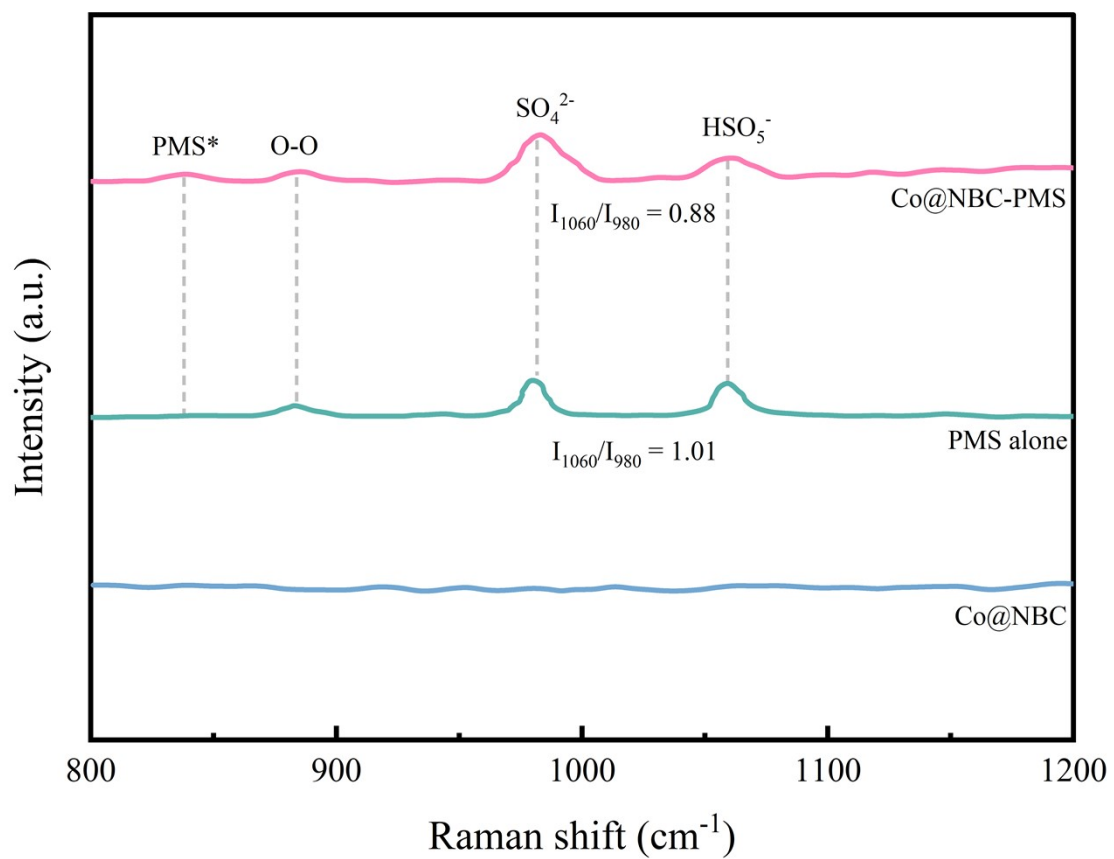**Fig. S12** Effect of concentration of MeOH on the removal rate of NOR in the Co@NBC-PMS system.
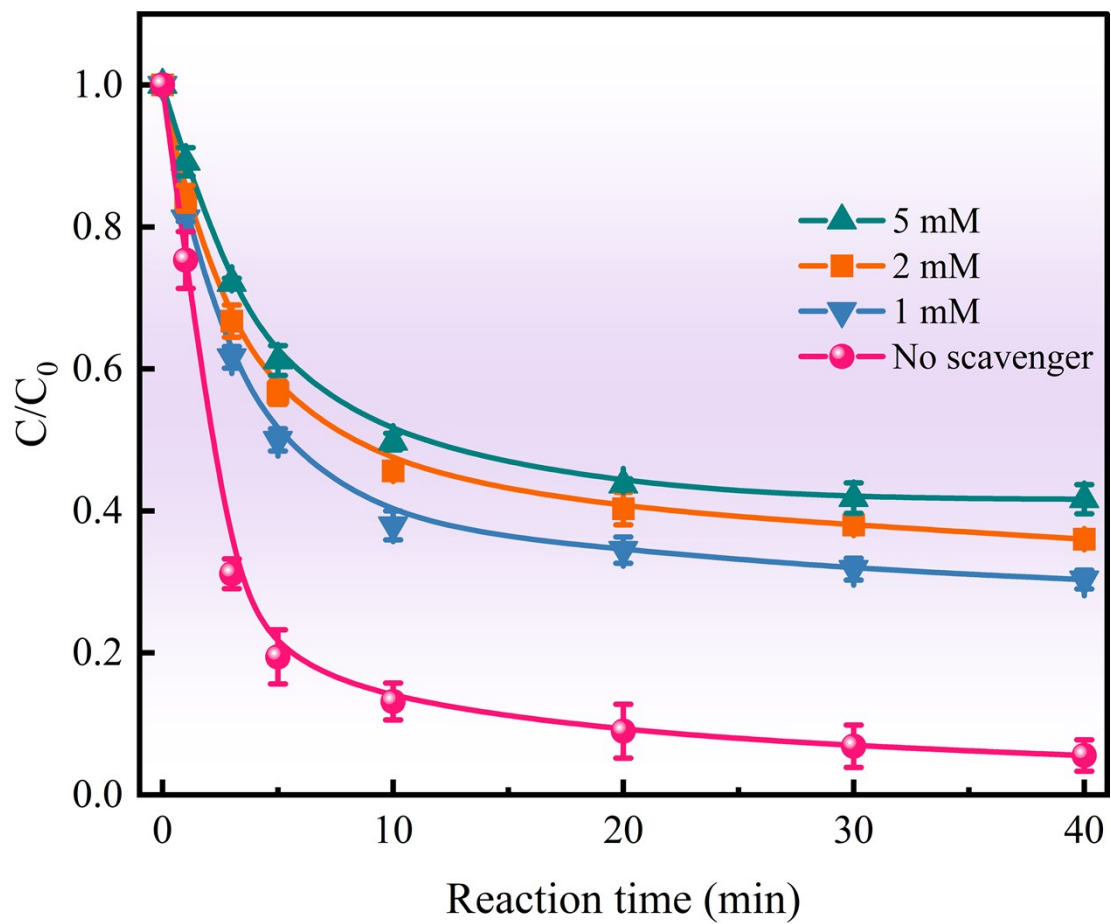
Fig. S13 Effect of concentration of p-BQ on the removal rate of NOR in the Co@NBC-PMS system.
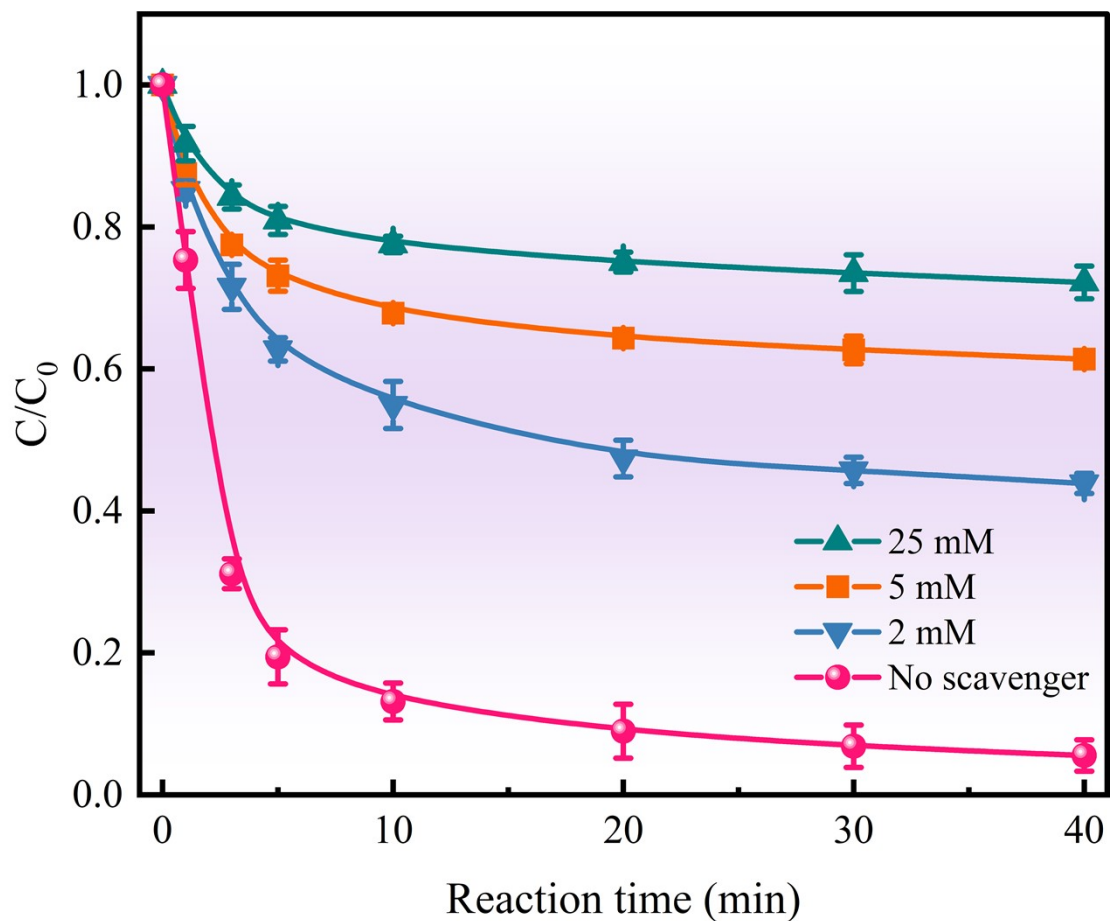
Fig. S14 Effect of concentration of L-his on the removal rate of NOR in the Co@NBC-PMS system.
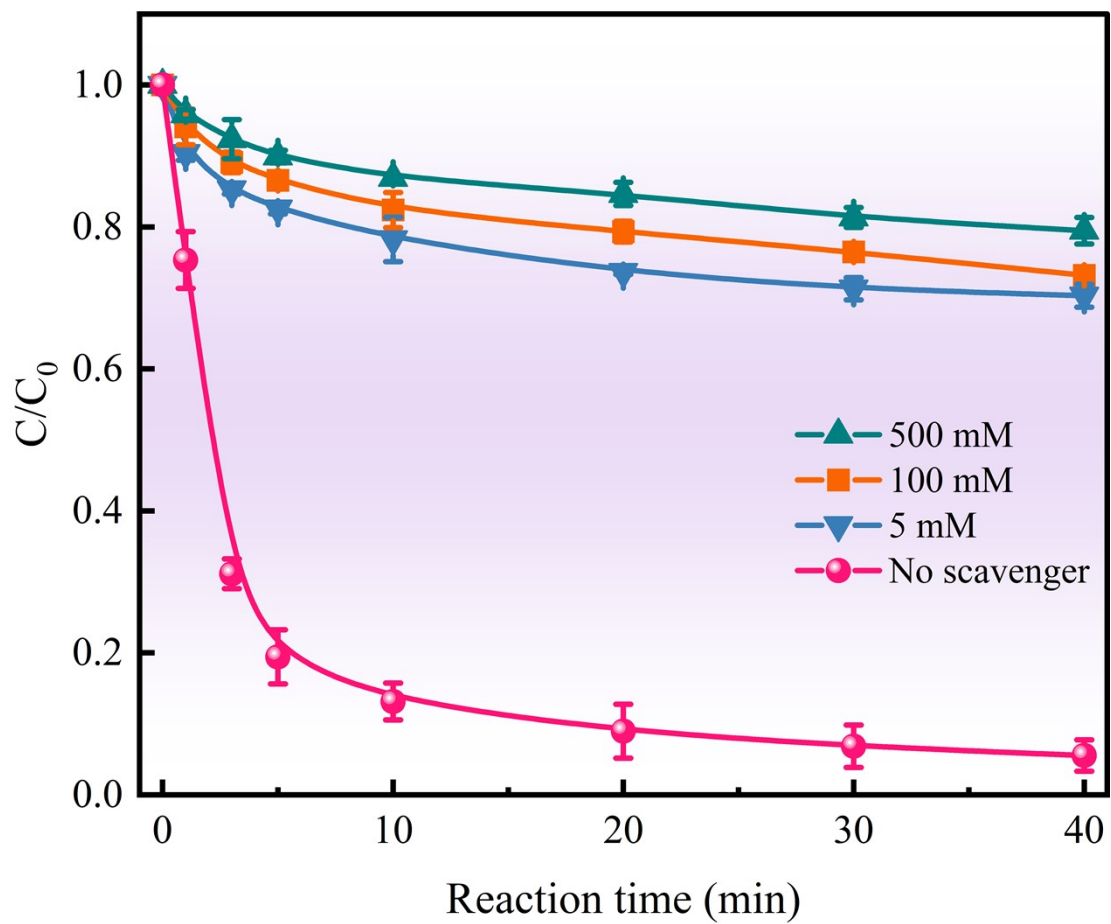
Fig. S15 Effect of concentration of FFA on the removal rate of NOR in the Co@NBC-PMS system.
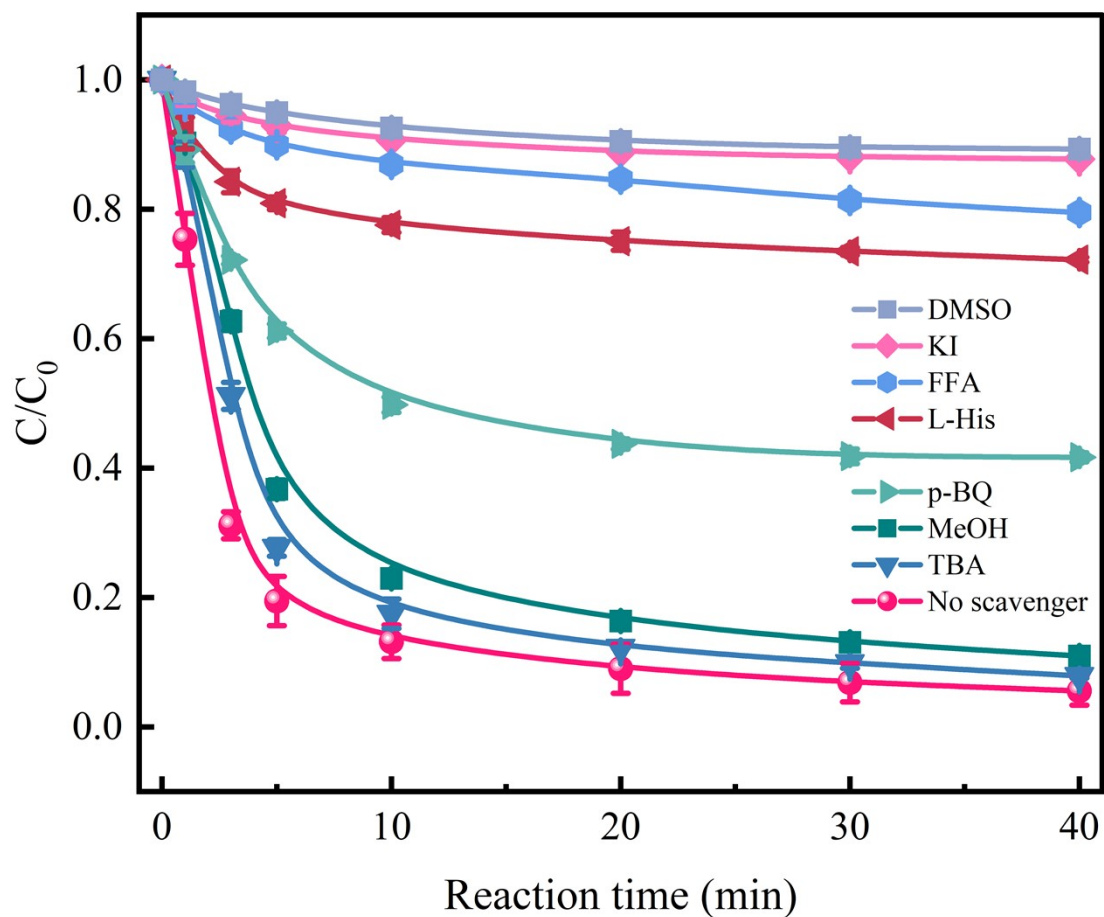
Fig. S16 Effect of different scavengers for the degradation of NOR in the Co@NBC-PMS system. (Reaction conditions: [TBA] = [MeOH] = [FFA] = 500 mM, [KI] = 50 mM, [L-his] = 25 mM, [p-BQ] = 5 mM, [DMSO] = 4 mM)
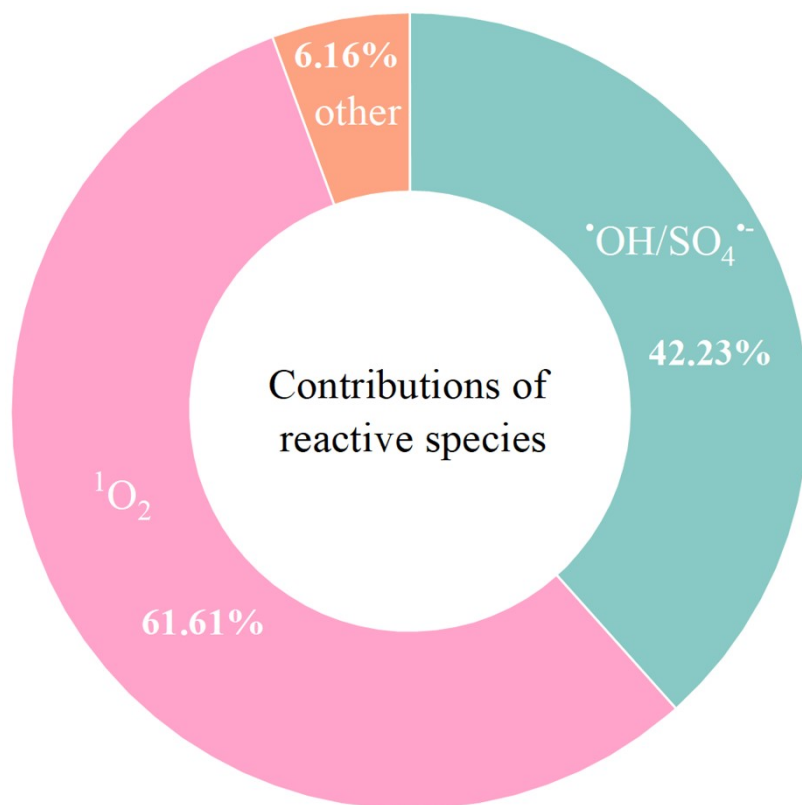
Fig. S17 Contributions of reactive species.
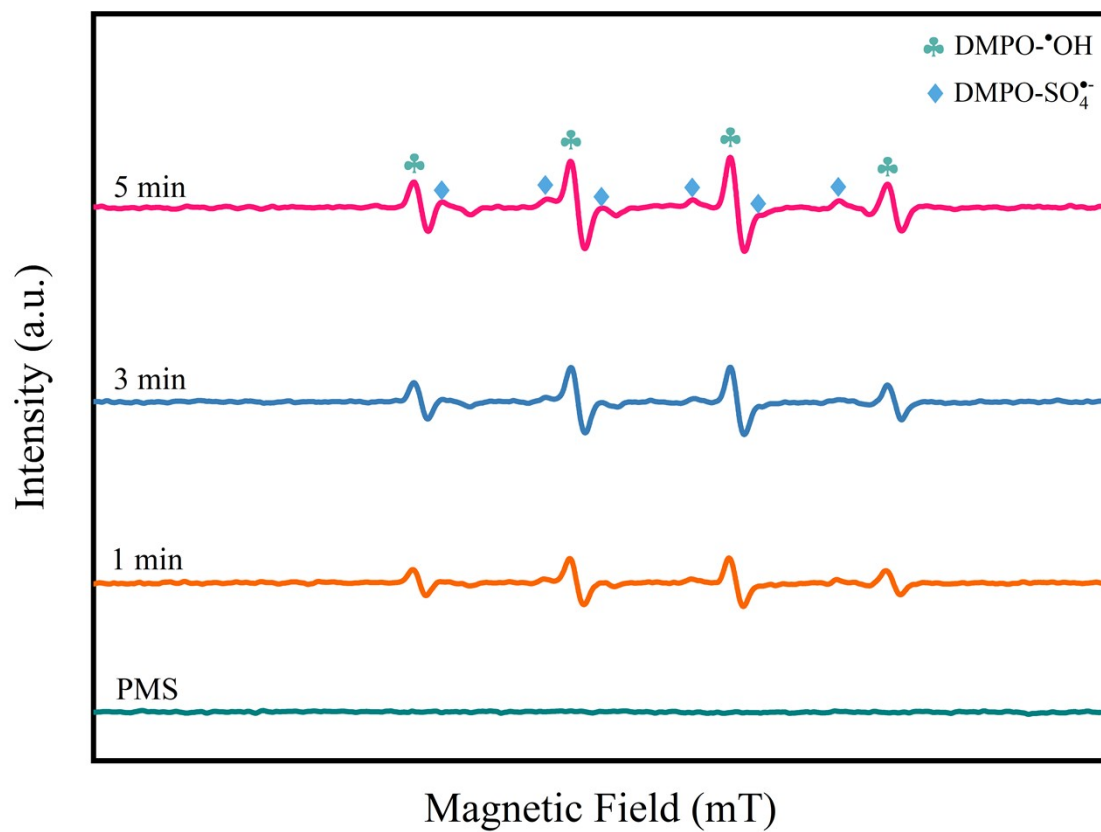
Fig. S18 EPR spectra with trapping agents of DMPO in the Co@NBC-PMS system.
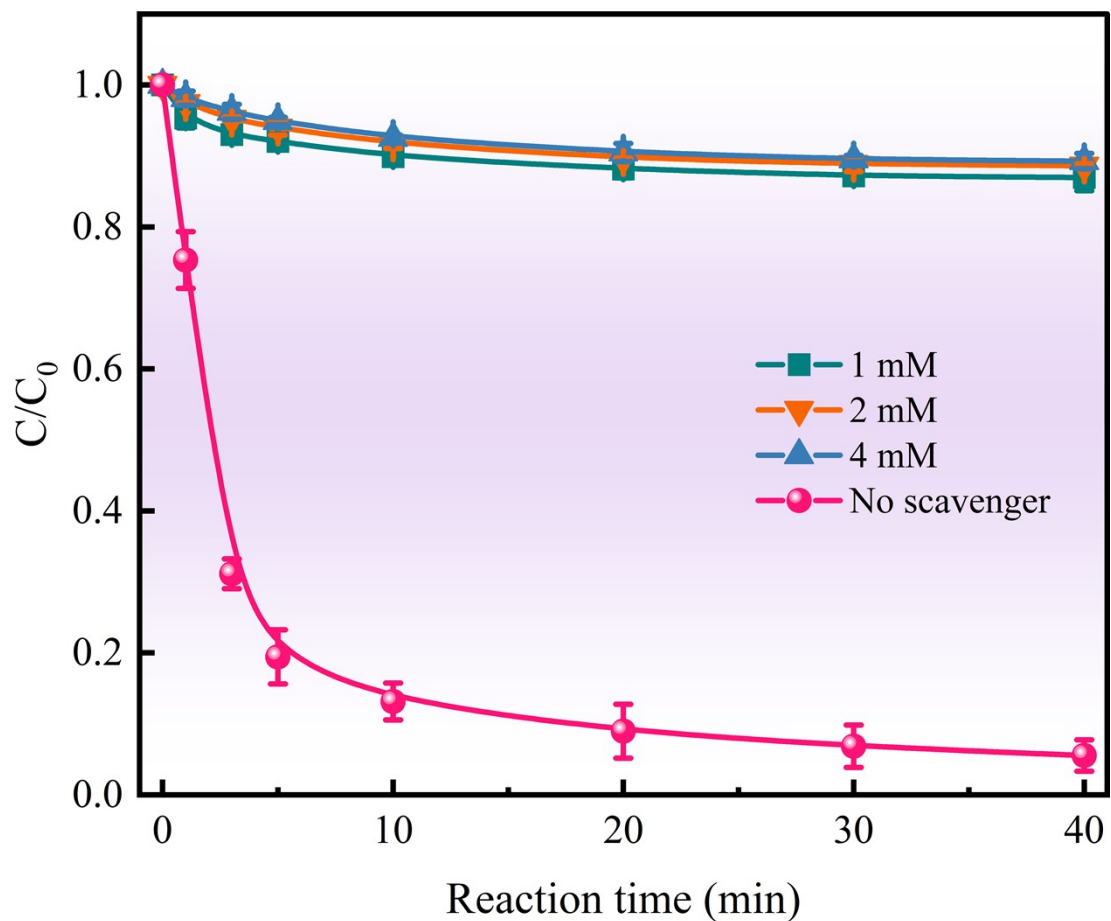
Fig. S19 Effect of concentration of DMSO on the removal rate of NOR in the Co@NBC-PMS system.

Fig. S20 Effect of concentration of KI on the removal rate of NOR in the Co@NBC-PMS system.

Fig. S21 In-situ Raman spectra of Co@NBC, PMS, and Co@NBC-PMS in water.
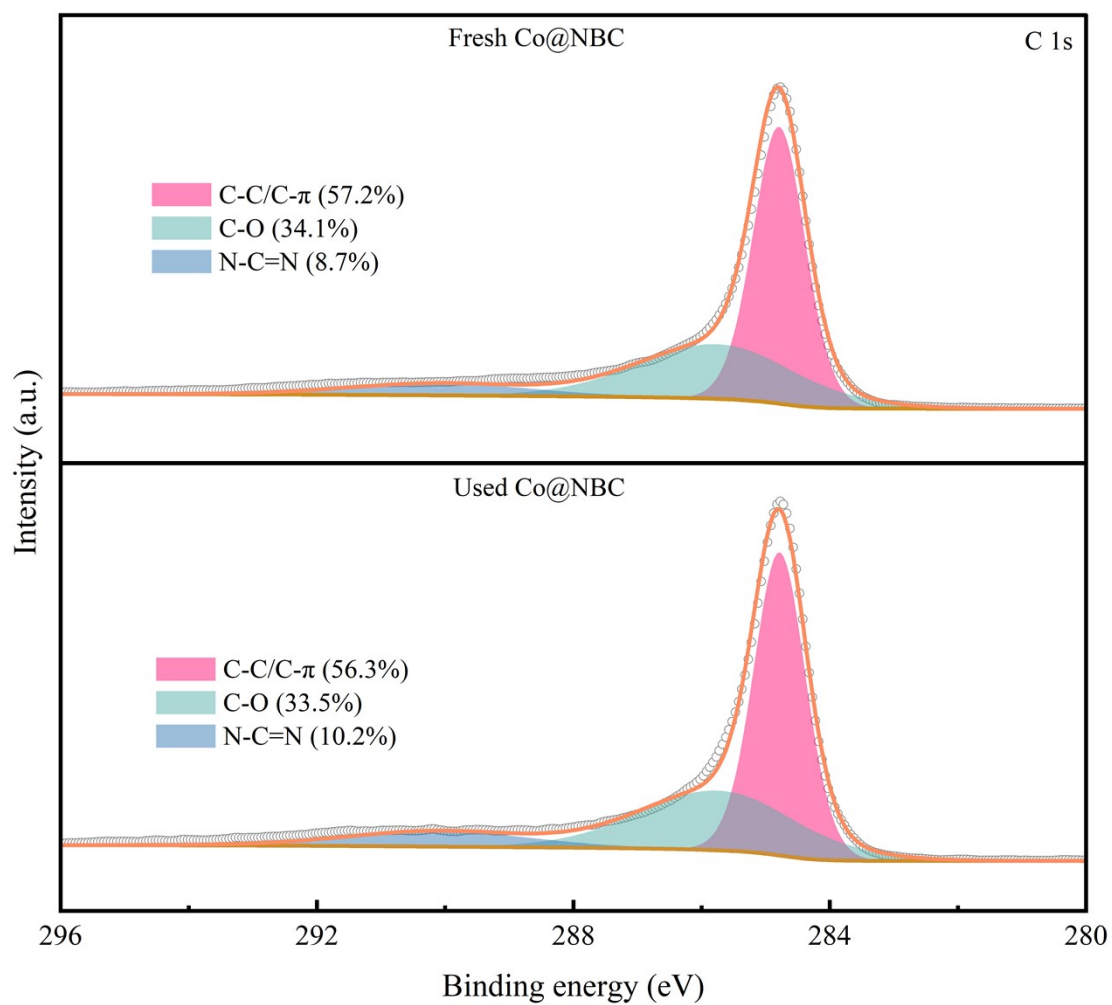
Fig. S22 C 1s XPS spectra of Co@NBC before and after use.
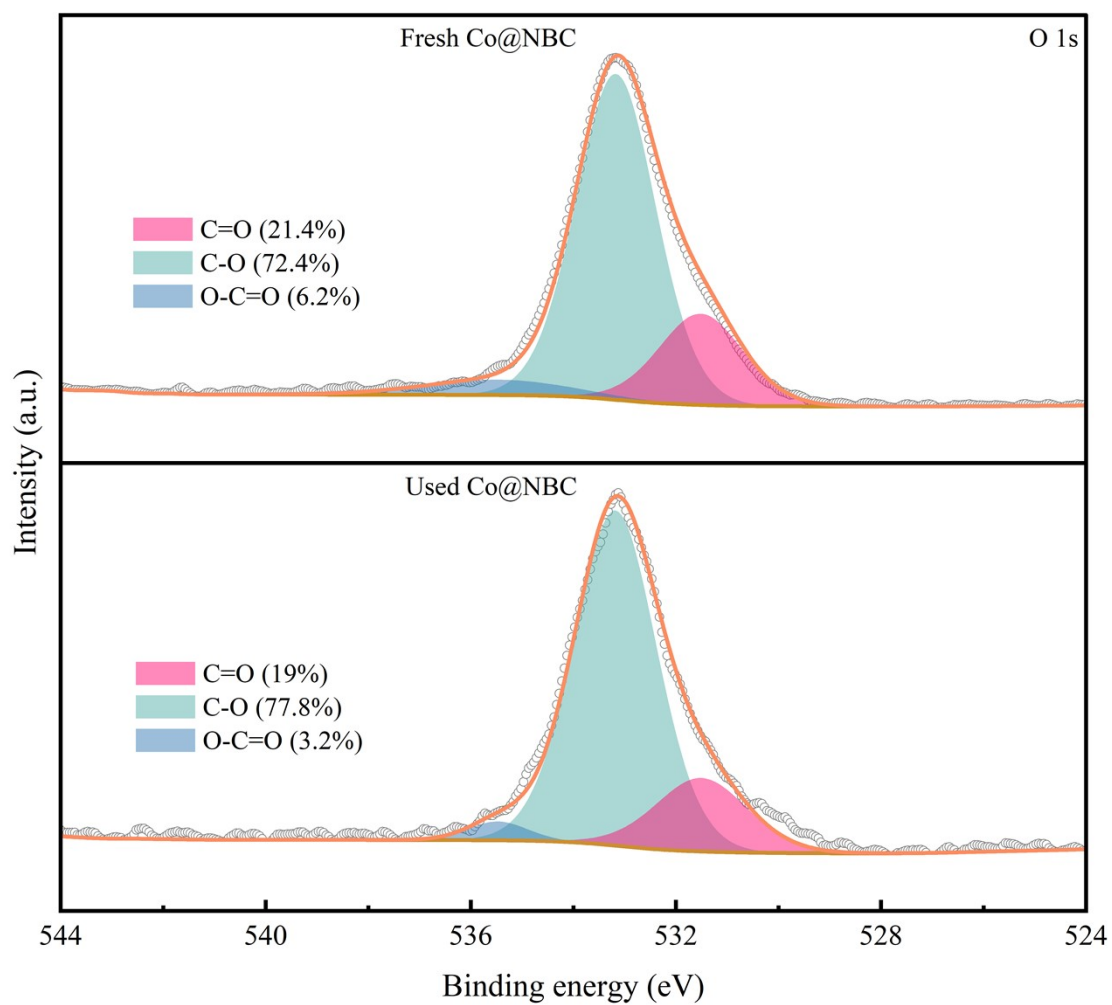
Fig. S23 O 1s XPS spectra of Co@NBC before and after use.
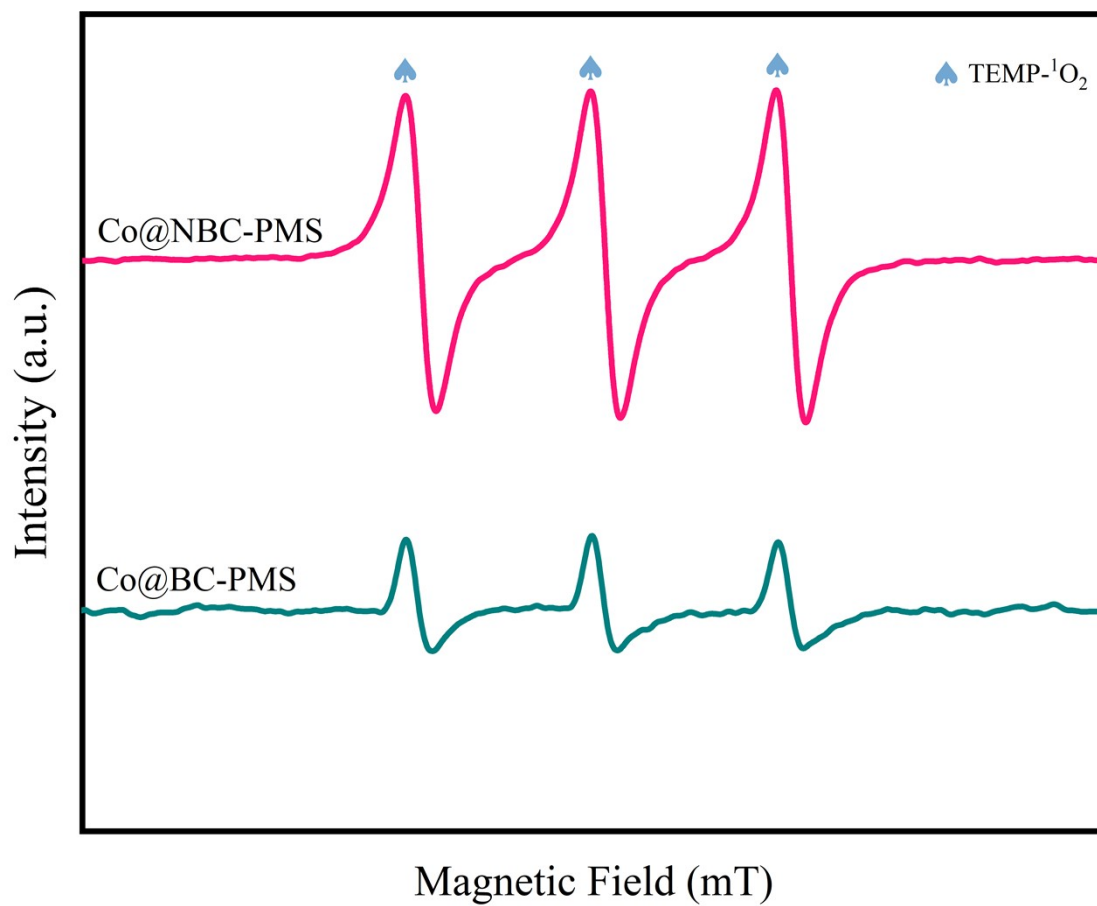
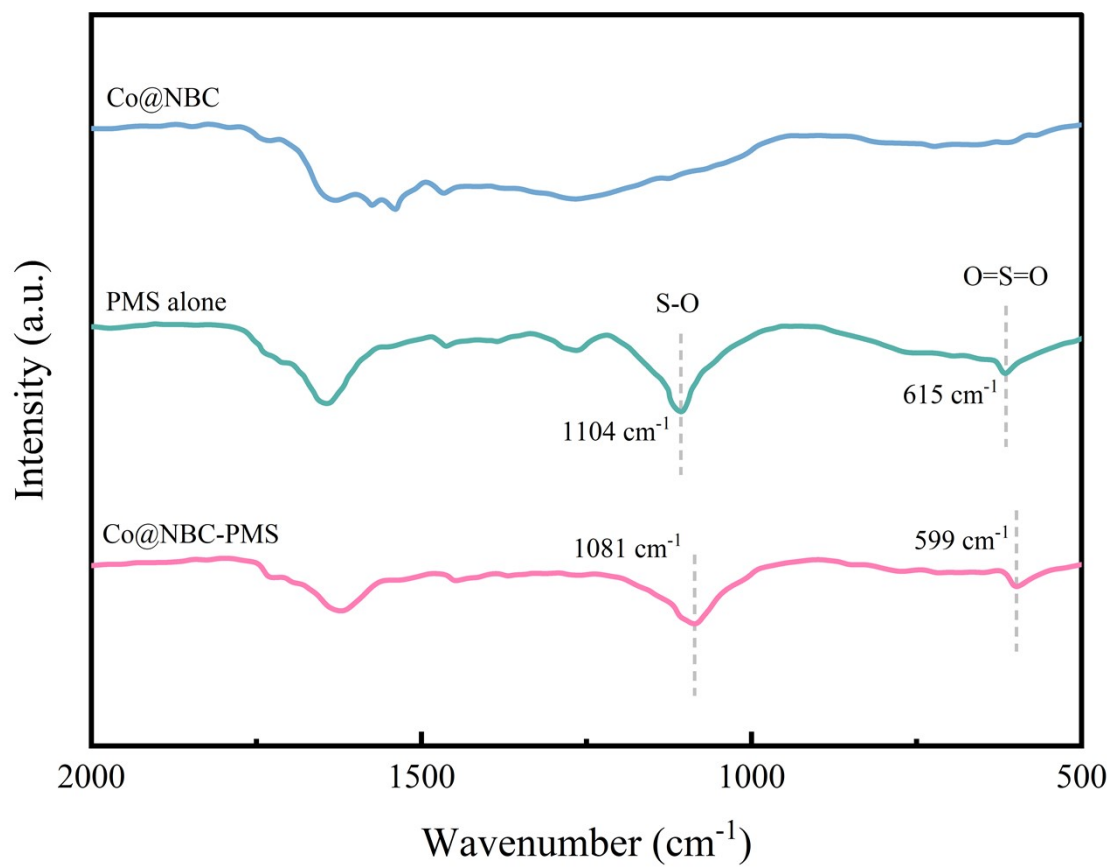**Fig. S24** EPR spectra with trapping agents of TEMP in the Co@NBC-PMS and Co@BC-PMS system.

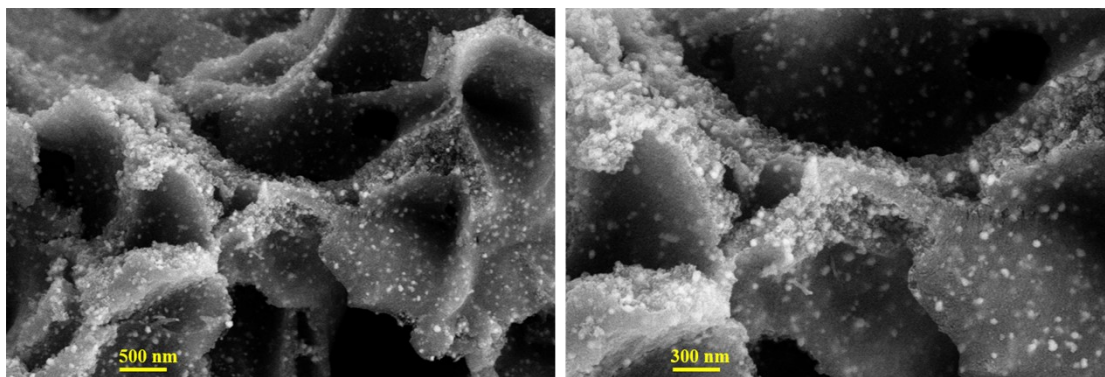**Fig. S25** In-situ FTIR spectra of Co@NBC, PMS, and Co@NBC-PMS in water.
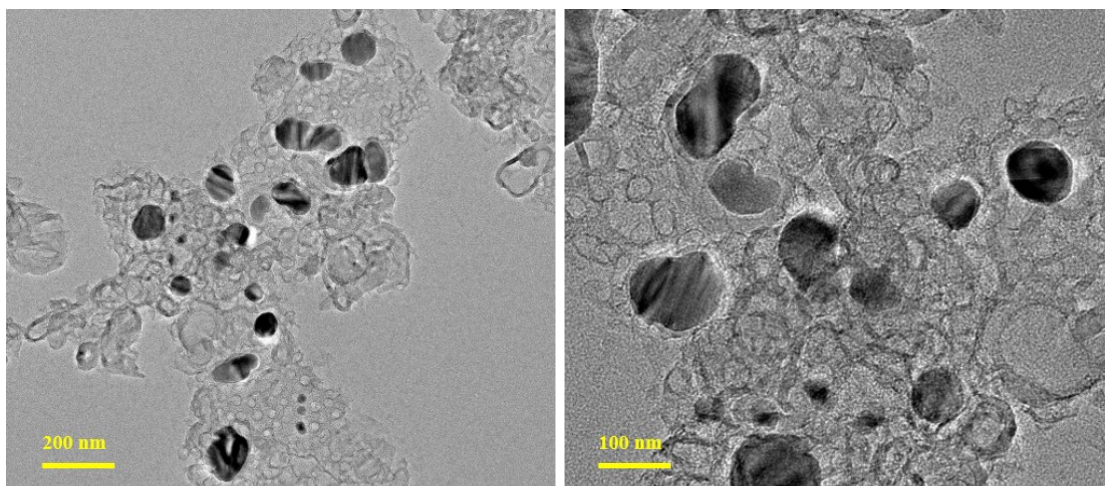
Fig. S26 SEM images of Co@NBC after 10 uses.

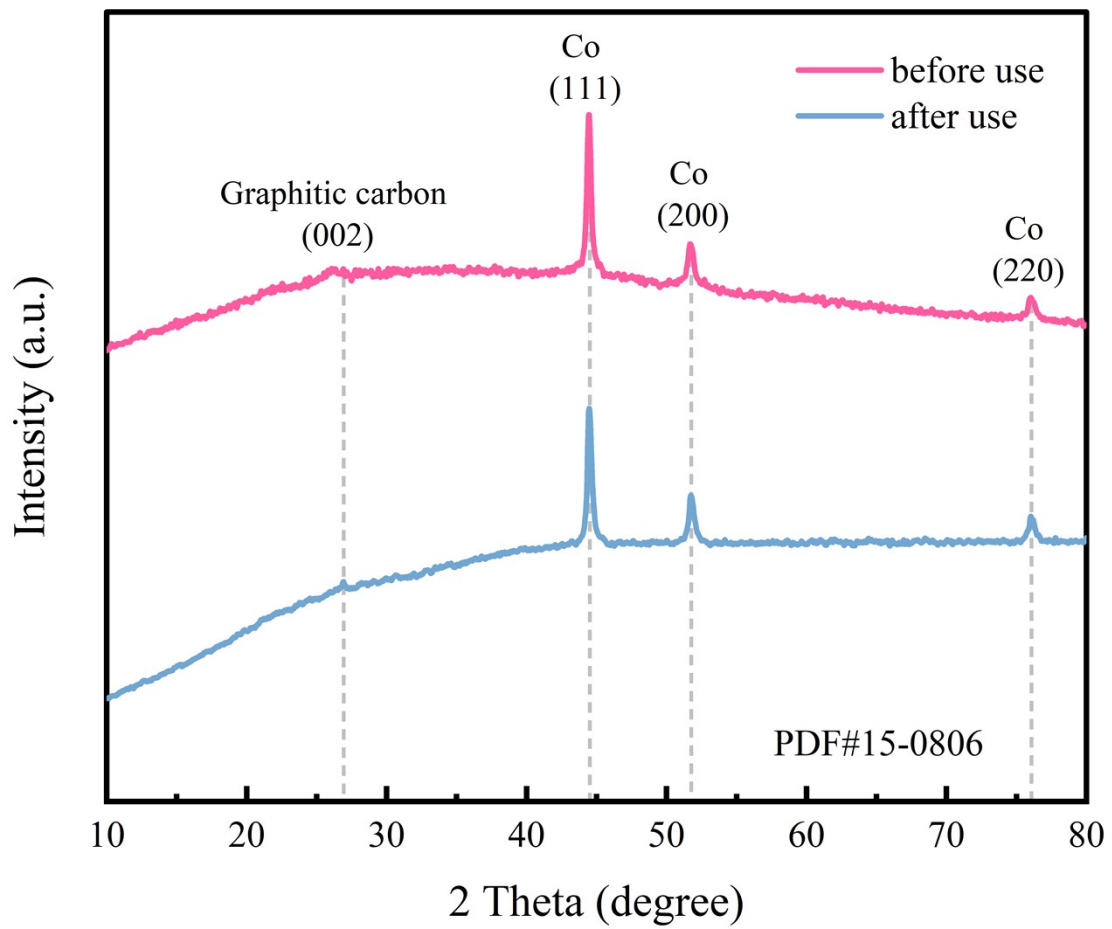**Fig. S27** TEM images of Co@NBC after 10 uses.

Fig. S28 XRD patterns of Co@NBC before and after use.
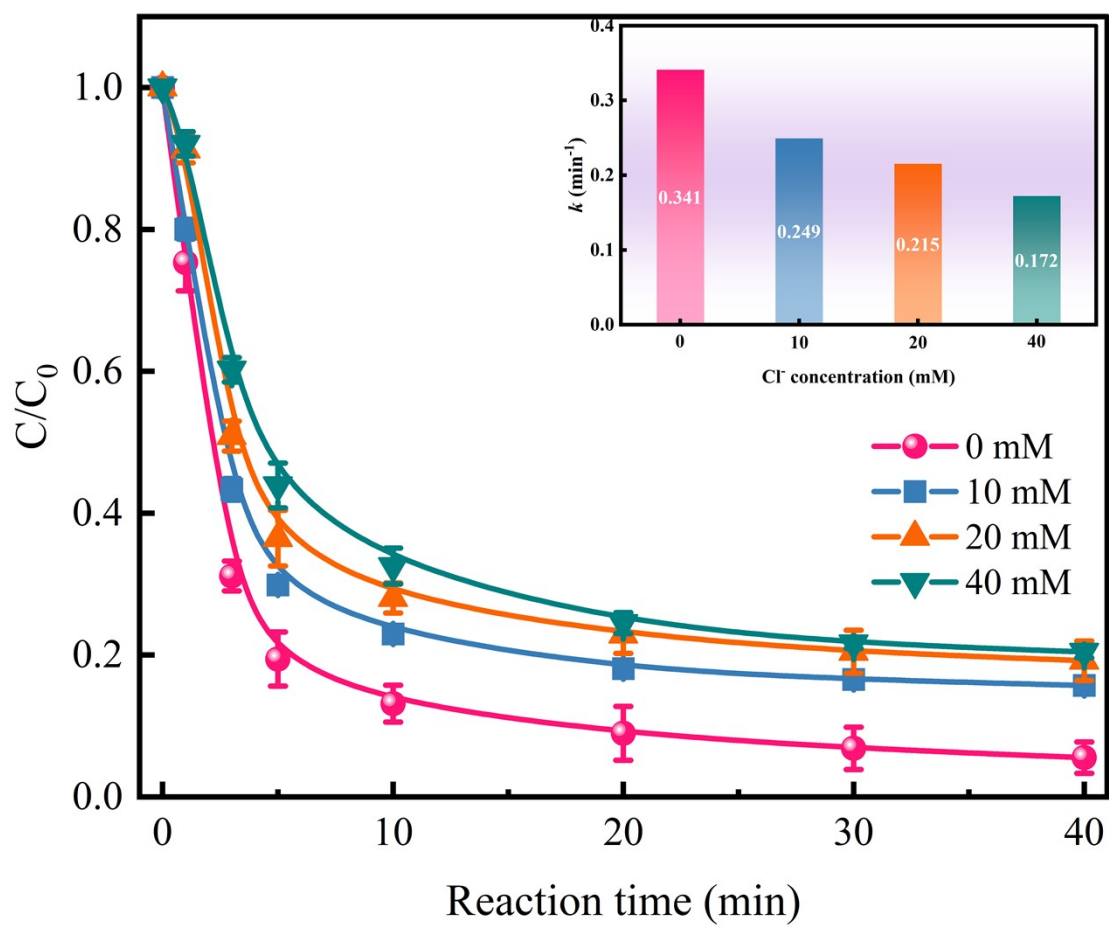
Fig. S29 Effect of Cl$^-$ on the removal rate of NOR in the Co@NBC-PMS system.
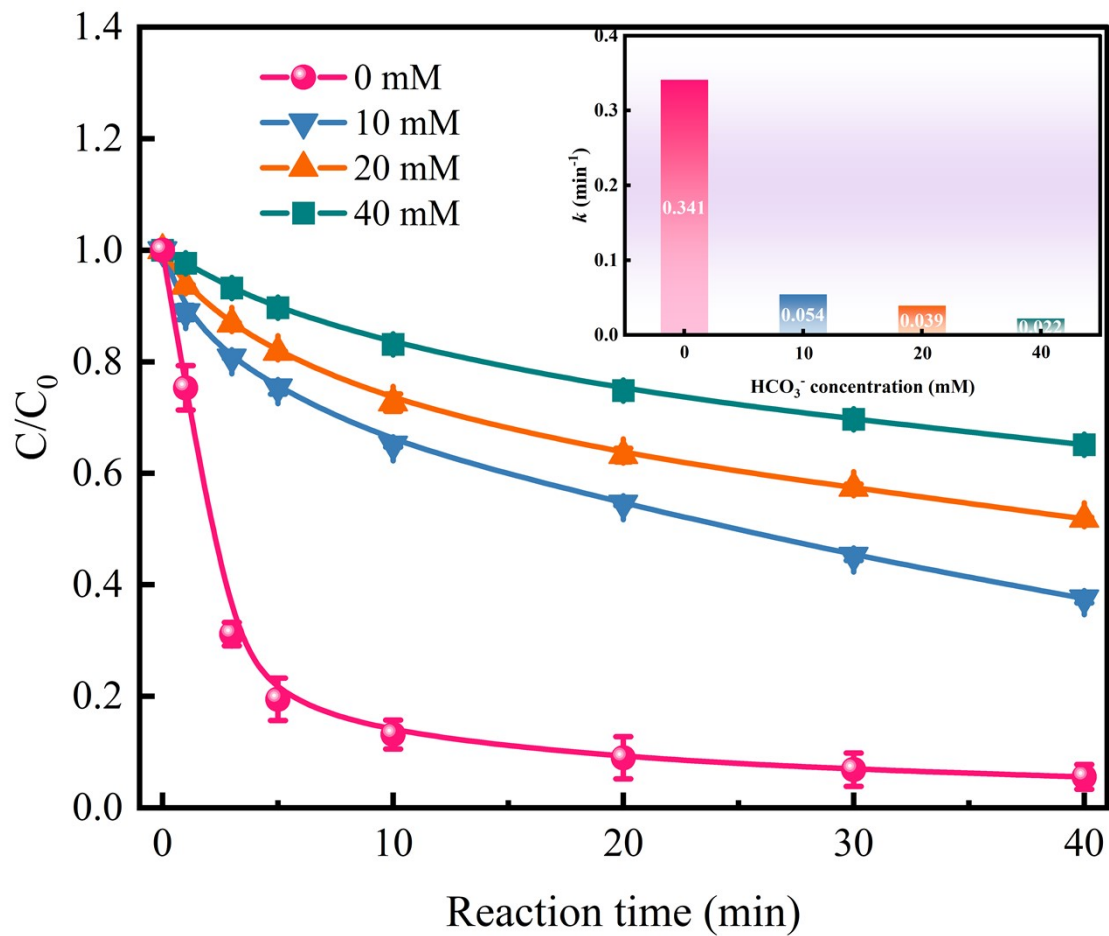
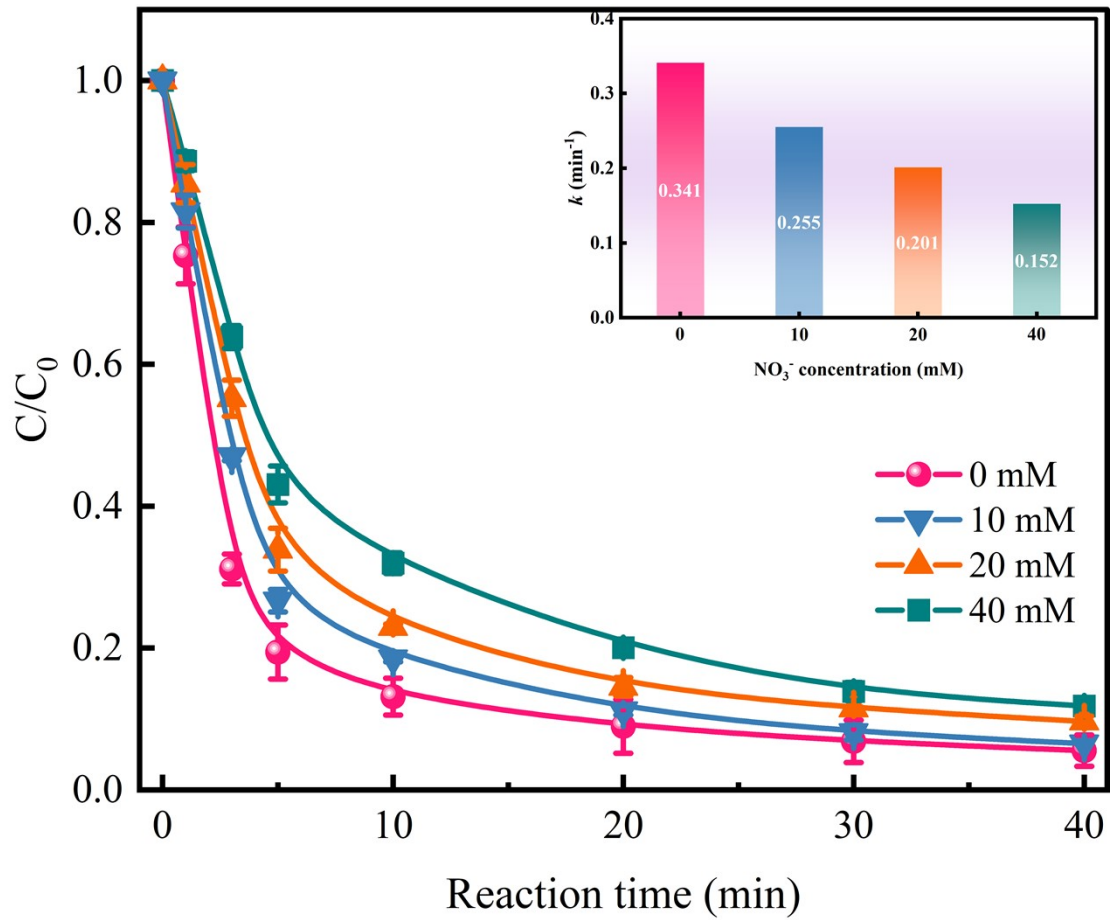**Fig. S30** Effect of HCO_3^- on the removal rate of NOR in the Co@NBC-PMS system.

Fig. S31 Effect of NO_3^- on the removal rate of NOR in the Co@NBC-PMS system.
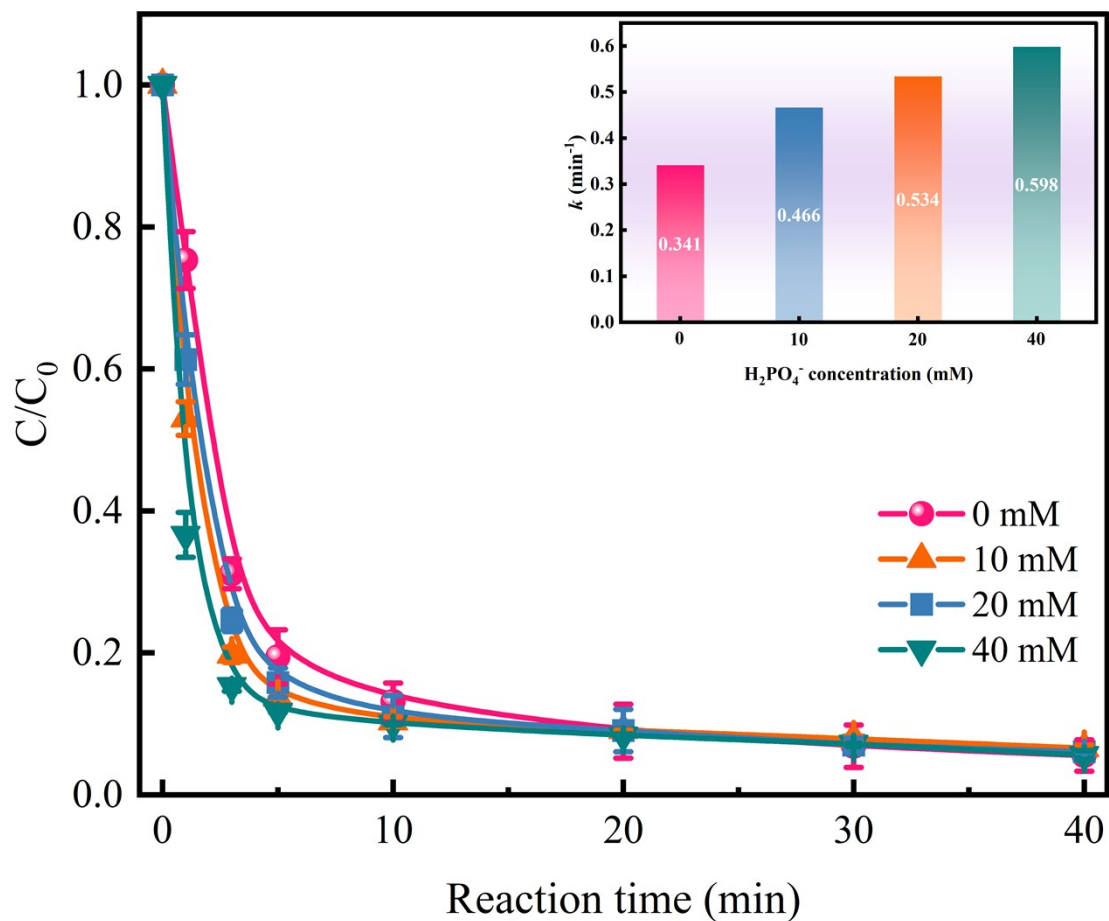
Fig. S32 Effect of $H_2PO_4^-$ on the removal rate of NOR in the Co@NBC-PMS system.

References

1 A.Wang, Y. Chen, Z. Zheng, H. Wang, X. Li, Z. Yang, R. Qiu, K. Yan, *Chem. Eng. J.,* 2021, **411**, 128497.

2 B. Liu, W. Guo, H. Wang, Q. Si, Q. Zhao, H. Luo, N. Ren, *J. Hazard. Mater.,* 2020, **398**, 122768.

3 Z. Wu, Z. Xiong, R. Liu, C. He, Y. Liu, Z. Pan, G. Yao, B. Lai, *J. Hazard. Mater.,* 2022, **427**, 128204.

4 C. Liang, C.F. Huang, N. Mohanty, R.M. Kurakalva, *Chemosphere,* 2008, **73**, 1540-1543.

5 Y. Wang, D. Tian, W. Chu, M. Li, X. Lu, *Sep. Purif. Technol.,* 2019, **212**, 536-544.

6 Y. Jing, M. Jia, Z. Xu, W. Xiong, Z. Yang, H. Peng, J. Cao, Y. Xiang, C. Zhang, *J. Hazard. Mater.,* 2022, **424**, 127503.

7 M. Xi, K. Cui, M. Cui, Y. Ding, Z. Guo, Y. Chen, C. Li, X. Li, *Chem. Eng. J.,* 2021, **420**, 129902.

8 T. Wang, M. Ta, J. Guo, L.-e. Liang, C. Bai, J. Zhang, H. Ding, *Sep. Purif. Technol.,* 2023, **304**, 122354.

9 M. Ta, T. Wang, J. Guo, Y. Wang, J. Zhang, C. Zhao, S. Liu, G. Liu, H. Yang, *Sep. Purif. Technol.,* 2023, **310**, 123067.

10 G. Wang, D. Zhao, F. Kou, Q. Ouyang, J. Chen, Z. Fang, *Chem. Eng. J.,* 2018, **351**, 747-755.

11 C. Zhang, K. Wang, K. Xie, X. Han, W. Ma, X. Li, G. Teng, *Chem. Eng. J.* 2022, **446**, 136907.

12 L. Gao, Y. Guo, J. Zhan, G. Yu, Y. Wang, *Water Res.,* 2022, **221**, 118730.

13 Y. Zhu, H. Ding, J. Fan, S. Liu, Y. Song, H. Deng, C. Zhao, D.D. Dionysiou, *ACS EST Eng.,* 2022, **2**(7), 1316-1325.

14 Y. Yang, G. Banerjee, G.W. Brudvig, J.H. Kim, J.J. Pignatello, *Environ. Sci. Technol.,* 2018, **52**(10), 5911-5919.